Progress in Earth and Planetary Science

RESEARCH ARTICLE | Open Access

Synoptic meteorological conditions of gamma-ray glows in winter thunderstorms

Yuuki Wada[1,2*], Miwa Tsurumi[2,3], Syugo Hayashi[4] and Koichiro Michimoto[5]

Abstract

The Gamma-ray Observation of Winter Thunderclouds collaboration has detected 70 gamma-ray glows, a high-energy phenomenon associated with thunderstorms, from October 2016 to March 2020 in Kanazawa and Komatsu, Ishikawa Prefecture, a central part of Japan facing the Sea of Japan. Based on surface and 500 hPa analyses, numerical prediction models, and surface and satellite observations, we classify their synoptic meteorological conditions into mainly three types. Most of the glow-detection cases were in west or west-southwest winds around the detection sites. Over half of the cases took place when a convex structure of surface pressure, often associated with a trough at 500 hPa, was formed along the coast of the Sea of Japan. Besides, we extract non-detection cases during winter thunderstorms in Kanazawa to compare with the glow-detection cases. While some of the non-detection cases have similar meteorological conditions as the glow-detection cases, most of the non-detection cases exhibited higher temperatures at the surface and 850 hPa, and higher − 10 °C altitudes, which indicates that electrification occurs at higher altitudes than the glow-detection cases. Therefore, gamma rays might have been produced but were attenuated before reaching the ground and undetectable at sea level.

Keywords Gamma-ray glow, Winter thunderstorm, High-energy atmospheric physics, Lightning discharge, Thundercloud

1 Introduction

Gamma-ray glows (also referred to as long bursts and thunderstorm ground enhancements: TGEs) are high-energy phenomena associated with thunderstorm activities. Gamma-ray glows are thought to originate from relativistic electrons inside thunderclouds. In strong electric fields of thunderclouds, electrons are accelerated by a scheme such as relativistic runaway electron avalanche (RREA: Gurevich et al. 1992) and modification of the cosmic-ray spectrum (MOS: Chilingarian et al. 2014) and emit bremsstrahlung photons by colliding with atmospheric atoms. While the first detections were made by airborne experiments (Parks et al. 1981; McCarthy and Parks 1985), most of the gamma-ray glows were detected by high-altitude ground-based experiments at Mt. Aragats in Armenia (Chilingarian et al. 2010, 2017, 2019), in Yangbajing in Tibet, China (Tsuchiya et al. 2012), at Tien Shan in Kazakhstan (Shepetov et al. 2021), in Puebla, Mexico (Bowers et al. 2019), at Lomnicky Stit in Slovak Republic (Chum et al. 2020), at Musala in Bulgaria (Chilingarian et al. 2021), at Mt. Norikura (Tsuchiya et al. 2009) and Mt. Fuji (Torii et al. 2009) in Japan.

Gamma-ray glows have been also detected at sea level during winter thunderstorms in Japan (Torii et al. 2002; Tsuchiya et al. 2007; Kuroda et al. 2016; Wada et al.

*Correspondence:
Yuuki Wada
wada@yuuki-wd.space
[1] Graduate School of Engineering, Osaka University, 2-1 Yamadaoka, Suita, Osaka 565-0871, Japan
[2] Extreme Natural Phenomena RIKEN Hakubi Research Team, Cluster of Pioneering Research, RIKEN, 2-1 Hirosawa, Wako, Saitama 351-0198, Japan
[3] Graduate School of Science and Engineering, Aoyama Gakuin University, 5-10-1 Fuchinobe, Sagamihara, Kanagawa 252-5258, Japan
[4] Meteorological Research Institute, Japan Meteorological Agency, 1-1 Nagamine, Tsukuba, Ibaraki 305-0052, Japan
[5] Independent Scholar, 2-44-11 Kosenba-machi, Kawagoe, Saitama 350-0036, Japan

2021a). Cold and dry air masses from Siberia are provided water vapor when crossing the Tsushima warm current, and then convective clouds with lightning discharges are produced and approach the coastal area of the Sea of Japan (Ishii et al. 2014). In general, gamma-ray photons are attenuated in the atmosphere within several hundreds of meters. For example, the average photon energy of gamma-ray glows is 2–3 MeV as derived with an average energy spectrum (Wada et al. 2021a), and the mean free path of 3 MeV photons is 220 m at sea-level. Therefore, gamma rays produced in summer thunderstorms hardly reach the ground because their charge center is typically above 3 km. To avoid the attenuation of gamma rays in the atmosphere, airborne experiments with aircrafts and balloons or ground-based observations at high altitudes are necessary for summertime thunderstorms. On the other hand, gamma-ray glows in winter thunderstorms can be detected even at sea-level because their charge center and the lower charge-layer edge can be at 1–2 km and at < 1 km, respectively, resulting in less attenuation of gamma rays in the atmosphere. The first detection in a winter thunderstorm was made by radiation monitors around the Monju Nuclear Power Plant, Fukui Prefecture (Torii et al. 2002). The Gamma-ray Observation of Winter Thunderclouds (GROWTH) collaboration started a dedicated gamma-ray observation at the Kashiwazaki-Kariwa nuclear power station, Niigata Prefecture (Tsuchiya et al. 2007, 2011, 2013), and then is operating an observation network with multiple gamma-ray monitors in Ishikawa Prefecture (Wada et al. 2018, 2019, 2021b; Yuasa et al. 2020). A total of 70 gamma-ray glows were detected in Ishikawa in four winter seasons from October 2016 to March 2020 (Wada et al. 2021a).

Winter thunderstorms have characteristics quite different from summer ones (Kitagawa and Michimoto 1994; Rakov and Uman 2003). (1) Charge center is frequently at 1–2 km, and the lower charge-layer edge can be at < 1 km. Thunderclouds in wintertime have a lower charge center because the altitude of $-10\,^{\circ}\mathrm{C}$ where the charge-separation process is thought to efficiently work gets closer to the ground (Kitagawa 1992; Kitagawa and Michimoto 1994; Yoshida et al. 2008; Takahashi et al. 2019). (2) Lightning discharges that release more than 100 C are occasionally observed (Brook et al. 1982; Suzuki 1992). (3) The ratio of positive cloud-to-ground discharges to negative ones is higher than in summertime (Takeuti et al. 1978; Brook et al. 1982; Ishii et al. 2014). (4) Lightning discharges are frequently initiated by upward leaders from tall ground objects (Miyake et al. 1990; Suzuki 1992). (5) The duration of thunderstorm activities is generally shorter and lightning flashes are less frequent than in the summertime. In particular, thunderstorms that exhibit only a few lightning flashes in their lifecycle are called "single-flash storms" (Michimoto 1993). Michimoto (1993) concluded that single-flash storms likely develop when the $-10\,^{\circ}\mathrm{C}$ altitude is between 1.4 and 1.8 km. The single-flash storms could be important for gamma-ray glows because they occur in the lower charge-center condition, and also quasi-stable electric fields that accelerate electrons are not interrupted frequently.

Synoptic conditions of winter storms in Japan have been investigated mainly from the perspective of heavy snowfalls. The conditions that bring snowfall to Japan are mainly classified into "coastal" and "mountainous" types (Fujita 1966; Iwamoto et al. 2008). The coastal snowfall type occurs when a trough or a cold-core low at the 500 hPa level develops over the Sea of Japan. A convex isobar structure develops at the ground surface, and westerly wind with a southern component is dominant. It snows mainly in the coastal areas of the Sea of Japan, and it can become disaster-level heavy snowfall when the Japan sea Polar air mass Convergence Zone (JPCZ) develops (Asai 1988; Eito et al. 2010; Tachibana et al. 2022). Winter thunderstorms develop typically in the coastal type (Goto and Narita 1991). When a 500 hPa trough or cold-core low passes over to the Pacific Ocean, the mountainous snowfall type develops. The surface pressure pattern becomes a dense isobar with a north-south run, which strengthens the northern winter monsoon. It provides heavy snowfalls mainly in inland mountainous areas due to the strong northern winds and mountainous geographical effects.

Wada et al. (2021b) analyzed 11 gamma-ray glows detected at Kanazawa University in Ishikawa, combined them with X-band radar and disdrometer observations, and revealed that gamma-ray glows were always accompanied by convective clouds with a radar echo of > 35 dBZ, and by precipitation of graupels. While microscale meteorological conditions of gamma-ray glows have been studied, synoptic conditions have never been discussed well. In particular, it remains unclear what types of synoptic conditions can create mesoscale conditions that facilitate glow detections at sea level. In the present study, we discuss synoptic meteorological conditions during 70 gamma-ray glows in winter thunderstorms reported by Wada et al. (2021a), by utilizing weather charts, observations, numerical models, and meteorological satellite images. We mainly refer to surface and 500 hPa meteorological charts to analyze positions of lows, fronts, and pressure patterns. The differences between glow-detection and non-detection cases are also investigated. Throughout the paper, time is described in UTC (universal coordinated time) unless otherwise noted.

2 Methods

We refer to 70 gamma-ray glows reported in Wada et al. (2021a). The event list is shown in Table 1. The glow events are divided into 24 groups based on detection time, in order to focus on synoptic conditions rather than microscopic ones. Cases 11, 18, 19, and 23 contain 5 or more glows, and they are intensively analyzed in the following section.

We utilize surface analysis charts (ASAS) published every 6 h by the Japan Meteorological Agency (JMA), 500 hPa constant-pressure charts (AUPQ35) published every 12 h by JMA, infrared satellite images of the Himawari-8 Advanced Himawari Imager (AHI) Band 13/TIR1, 10 min surface observations by JMA Automated Meteorological Data Acquisition System (AMeDAS), and mesoscale numerical prediction models (MSM) of JMA. The surface charts ASAS show isobaric lines of surface pressure in the unit of hPa, while the 500 hPa charts AUPQ35 show those of 500 hPa altitude in the unit of meter. A typical altitude of 500 hPa is $\sim$ 5500 m. The infrared satellite images of Himawari-8 provide brightness temperatures every 10 minutes with geolocation correction (Takenaka et al. 2020; Yamamoto et al. 2020), whose grid resolution is 0.02°. MSM is published every 3 h, covers N22.4°–N47.6° and E120°–E150° with a resolution of 0.1° (latitude) and 0.125° (longitude), and contains 39 h or 51 h predictions for the surface (1 h interval) and high altitudes (3 h intervals). In this study, initial analysis data of temperature and geopotential height are utilized, and prediction data are not employed. We mainly refer to these values at 850 hP altitude. The geopotential height at 850 hPa is typically $\sim$ 1500 m, where convections inside winter thunderclouds are active. The temperature at 850 hPa is a common parameter for weather forecasts. Average lapse rates between surface and 850 hPa height are also calculated with surface temperature, temperature, and geopotential height at 850 hPa. Also, the altitude at − 10 °C is calculated with MSM.

The observation sites of the GROWTH collaborations are roughly separated into two areas: Kanazawa and Komatsu. The two areas are $\sim$ 25 km apart, as shown in Fig. 1. We refer to the Kanazawa AMeDAS station (N36.588°, E136.633°) and the Komatsu AMeDAS station (N36.382°, E136.435°) for surface observations of temperature. The AMeDAS stations are shown in Fig. 1. We also extract the temperature at 850 hPa and the lapse rate between the surface and 850 hPa with the MSM data, as mentioned above. Its base location is N36.6°, E136.625° and N36.4°, E136.5° for the Kanazawa and Komatsu areas, respectively.

The wind direction and speed at the moment of glows are retrieved from Wada et al. (2021a), estimated by pattern matching of X-band radar images. The region of the wind estimation is N36.4°–36.7°, E136.4°–136.8° for Kanazawa, and N36.25°–36.55°, E136.2°–136.6° for Komatsu. Considering the elevation angle of the X-band radar, the estimated wind information is at $\sim$ 1 km altitude. The wind direction is where the wind comes in clockwise. For example, 0°, 90°, 180°, and 270° indicate that winds blow from north to south, from east to west, from south to north, and from west to east, respectively.

To investigate the lightning occurrence, we utilize the LIghtning DEtection Network system (LIDEN) of JMA (Ishii et al. 2014). Based on the LIDEN data, we produce daily lightning maps around Ishikawa Prefecture and calculate flash rates. The flash rate corresponding to a glow is calculated as follows: We count total lightning flashes (both cloud-to-ground and in-cloud flashes) from 5 minutes before to 5 minutes after the glow detection in a 20 km×20 km region centered at the detection site. Then, the number of flashes is divided by 10 minutes. If a lightning flash consists of multiple strokes, we consider the position of the flash to be that of the first stroke.

Besides the glow-detection cases, this study also analyzes conditions that exhibit winter thunderstorms but no gamma-ray glows. We focus on non-detection cases in Kanazawa because Kanazawa has more gamma-ray monitors than Komatsu. The criterion of non-detection cases is when gamma-ray monitors in Kanazawa were in operation but no gamma-ray glows were detected, and when the Kanazawa local meteorological observatory of JMA reported lightning activities within 10 km of the observatory. The extracted non-detection cases are also confirmed with the daily lightning maps of LIDEN. We exclude the 2016–2017 winter seasons because of fewer gamma-ray monitors than in other seasons. The wind direction and speed are estimated with the X-band radar images as the same method as Wada et al. (2021a). Note that the X-band radar was not in operation during the non-detection case 9, and instead C-band radar images of JMA are utilized for the wind estimation. The flash rates of the non-detection cases are extracted in the same way as the glow cases, with a 10 min window and a 20 km×20 km region centered at the local observatory. We employ the maximum rate during the non-detection period.

3 Results

3.1 Glow-detection cases

In this section, we first analyze Cases 11, 18, 19, and 23, which include 5 or more gamma-ray glows, based on surface and 500 hPa analyses, and satellite images. The other cases are then analyzed. The list of gamma-ray glows is presented in Table 1.

Table 1 List of gamma-ray glows recorded in Kanazawa and Komatsu areas

Case no.	Event no.	Detection time (UTC)	Area	Temperature		Lapse rate (°C/km)	Altitude at −10 °C (km)	Wind		Flash rate (flash/min)
				Ground (°C)	850 hPa (°C)			Direction (°)	Speed (m/s)	
1	1	2016/12/07 15:13	Kanazawa	7.2	− 2.4	6.6	2.6	260	9.5	0.0
	2	2016/12/07 17:56	Komatsu	5.9	− 3.2	6.3	2.4	300	10.9	0.0
	3	2016/12/07 17:58	Komatsu	5.9	− 3.2	6.3	2.4	300	10.9	0.0
2	4	2016/12/09 07:29	Kanazawa	9.7	0.2	6.7	2.8	260	18.1	0.3
3	5	2017/01/12 16:43	Kanazawa	5.7	− 5.8	8.6	1.9	260	20.1	0.7
	6	2017/01/12 20:05	Kanazawa	6.1	− 6.0	9.0	1.9	270	16.1	0.3
4	7	2017/01/14 20:30	Kanazawa	− 0.4	− 11.8	8.4	1.2	310	16.7	0.0
5	8	2017/02/05 20:06	Kanazawa	6.8	− 3.8	7.9	2.3	260	16.5	0.3
	9	2017/02/05 20:10	Kanazawa	6.8	− 3.8	7.9	2.3	260	16.5	0.2
6	10	2017/12/04 18:27	Komatsu	6.8	− 3.8	7.6	2.3	250	13.2	0.2
	11	2017/12/04 18:27	Komatsu	6.8	− 3.8	7.6	2.3	250	13.2	0.2
7	12	2017/12/05 02:51	Kanazawa	5.0	− 3.9	6.4	2.2	240	20.2	0.9
	13	2017/12/05 03:07	Komatsu	4.0	− 4.0	5.8	2.2	240	21.6	0.0
	14	2017/12/05 09:33	Kanazawa	6.6	− 5.9	9.1	2.0	260	14.8	0.2
8	15	2017/12/11 08:49	Kanazawa	4.9	− 7.1	8.8	1.8	250	21.6	0.0
	16	2017/12/11 08:49	Kanazawa	4.9	− 7.1	8.8	1.8	250	21.6	0.0
	17	2017/12/11 08:52	Kanazawa	4.9	− 7.1	8.8	1.8	250	21.6	0.0
	18	2017/12/11 09:17	Kanazawa	4.0	− 7.1	8.1	1.8	250	21.0	0.0
9	19	2017/12/25 23:10	Kanazawa	5.8	− 5.8	8.2	2.0	260	20.6	0.0
	20	2017/12/25 23:11	Kanazawa	5.8	− 5.8	8.2	2.0	260	20.6	0.0
10	21	2018/01/02 18:19	Kanazawa	2.7	− 9.5	8.6	1.5	290	11.8	0.1
11	22	2018/01/09 14:41	Komatsu	1.8	− 6.6	6.2	1.8	250	15.9	0.0
	23	2018/01/09 17:36	Komatsu	1.6	− 6.9	6.2	1.8	250	20.4	0.0
	24	2018/01/09 17:53	Kanazawa	2.0	− 6.5	6.3	1.8	250	19.3	0.5
	25	2018/01/09 17:54	Kanazawa	2.0	− 6.5	6.3	1.8	250	19.3	0.5
	26	2018/01/09 17:57	Kanazawa	2.2	− 6.5	6.4	1.8	250	19.3	0.2
12	27	2018/01/09 22:34	Komatsu	1.6	− 7.1	6.3	1.8	250	16.1	0.0
	28	2018/01/10 02:59	Kanazawa	2.2	− 6.1	6.0	1.9	250	13.8	0.4
	29	2018/01/10 03:02	Kanazawa	2.2	− 6.1	6.0	1.9	250	13.8	0.7
13	30	2018/01/11 01:40	Kanazawa	− 0.4	− 10.1	6.9	1.4	240	18.2	0.2
14	31	2018/01/13 03:01	Kanazawa	1.2	− 7.8	6.2	1.7	260	10.8	0.0
	32	2018/01/13 03:01	Kanazawa	1.2	− 7.8	6.2	1.7	260	10.8	0.0
15	33	2018/01/23 04:29	Komatsu	3.2	− 6.4	7.0	1.8	250	25.6	0.0
16	34	2018/02/03 18:50	Kanazawa	1.1	− 8.6	6.9	1.6	250	13.8	0.2
17	35	2018/12/08 11:53	Kanazawa	5.1	− 6.8	8.1	1.9	250	14.0	0.0

Table 1 (continued)

Case no.	Event no.	Detection time (UTC)	Area	Temperature		Lapse rate (°C/km)	Altitude at − 10 °C (km)	Wind		Flash rate (flash/min)
				Ground (°C)	850 hPa (°C)			Direction (°)	Speed (m/s)	
	36	2018/12/08 12:09	Kanazawa	5.5	− 6.8	8.4	1.9	250	14.0	0.0
	37	2018/12/08 12:10	Kanazawa	5.5	− 6.8	8.4	1.9	250	14.0	0.0
18	38	2018/12/17 09:51	Kanazawa	7.7	− 2.2	7.1	2.6	270	10.9	0.9
	39	2018/12/17 09:54	Kanazawa	7.7	− 2.2	7.1	2.6	270	10.9	1.1
	40	2018/12/17 09:54	Kanazawa	7.7	− 2.2	7.1	2.6	270	10.9	1.1
	41	2018/12/17 10:15	Kanazawa	5.9	− 2.2	5.8	2.6	270	10.6	0.0
	42	2018/12/17 10:15	Kanazawa	5.9	− 2.2	5.8	2.6	270	10.6	0.0
	43	2018/12/17 14:15	Kanazawa	8.4	− 4.2	9.0	2.2	280	11.3	0.0
	44	2018/12/17 14:17	Kanazawa	8.4	− 4.2	9.0	2.2	280	11.3	0.0
19	45	2018/12/18 14:40	Kanazawa	8.1	− 4.7	8.8	2.2	270	13.5	1.3
	46	2018/12/18 14:42	Kanazawa	8.1	− 4.7	8.8	2.2	270	13.5	1.3
	47	2018/12/18 14:42	Kanazawa	8.1	− 4.7	8.8	2.2	270	13.5	1.1
	48	2018/12/18 14:42	Kanazawa	8.1	− 4.7	8.8	2.2	270	13.5	1.1
	49	2018/12/18 14:49	Kanazawa	6.6	− 4.7	7.7	2.2	270	11.9	1.3
	50	2018/12/18 14:51	Kanazawa	6.6	− 4.7	7.7	2.2	270	11.9	1.0
20	51	2019/01/21 15:51	Kanazawa	5.6	− 5.7	8.0	2.0	280	14.2	1.1
	52	2019/01/21 16:03	Kanazawa	4.2	− 5.7	7.0	2.0	270	13.6	0.4
21	53	2019/01/25 11:43	Kanazawa	2.8	− 4.5	5.2	2.1	260	16.9	0.1
	54	2019/01/25 11:44	Kanazawa	2.8	− 4.5	5.2	2.1	260	16.9	0.1
22	55	2020/01/12 17:03	Kanazawa	6.2	− 2.6	6.3	2.5	240	16.4	0.7
	56	2020/01/12 17:03	Kanazawa	6.2	− 2.6	6.3	2.5	240	16.4	0.7
	57	2020/01/12 17:05	Kanazawa	6.2	− 2.6	6.3	2.5	240	16.4	0.5
	58	2020/01/12 17:06	Kanazawa	6.2	− 2.6	6.3	2.5	240	16.4	0.4
23	59	2020/02/17 11:52	Kanazawa	2.5	− 6.9	6.9	1.8	260	15.7	0.1
	60	2020/02/17 12:00	Kanazawa	2.4	− 6.9	6.9	1.8	260	15.7	0.0
	61	2020/02/17 12:47	Kanazawa	2.6	− 6.9	7.0	1.8	250	15.0	0.0
	62	2020/02/17 12:49	Kanazawa	2.6	− 6.9	7.0	1.8	250	15.0	0.0
	63	2020/02/17 12:49	Kanazawa	2.6	− 6.9	7.0	1.8	250	15.0	0.0
	64	2020/02/17 12:51	Kanazawa	2.6	− 6.9	7.0	1.8	250	15.0	0.0
	65	2020/02/17 12:52	Kanazawa	2.6	− 6.9	7.0	1.8	250	15.0	0.0
	66	2020/02/17 12:53	Kanazawa	2.6	− 6.9	7.0	1.8	250	15.0	0.0
	67	2020/02/17 16:29	Kanazawa	1.1	− 7.0	6.0	1.8	260	12.7	0.2
	68	2020/02/17 16:30	Kanazawa	1.1	− 7.7	6.5	1.7	260	12.7	0.2
	69	2020/02/17 16:35	Komatsu	1.9	− 7.5	6.9	1.7	260	13.6	0.1
24	70	2020/03/15 21:28	Kanazawa	4.1	− 6.1	7.6	1.8	280	13.0	0.3

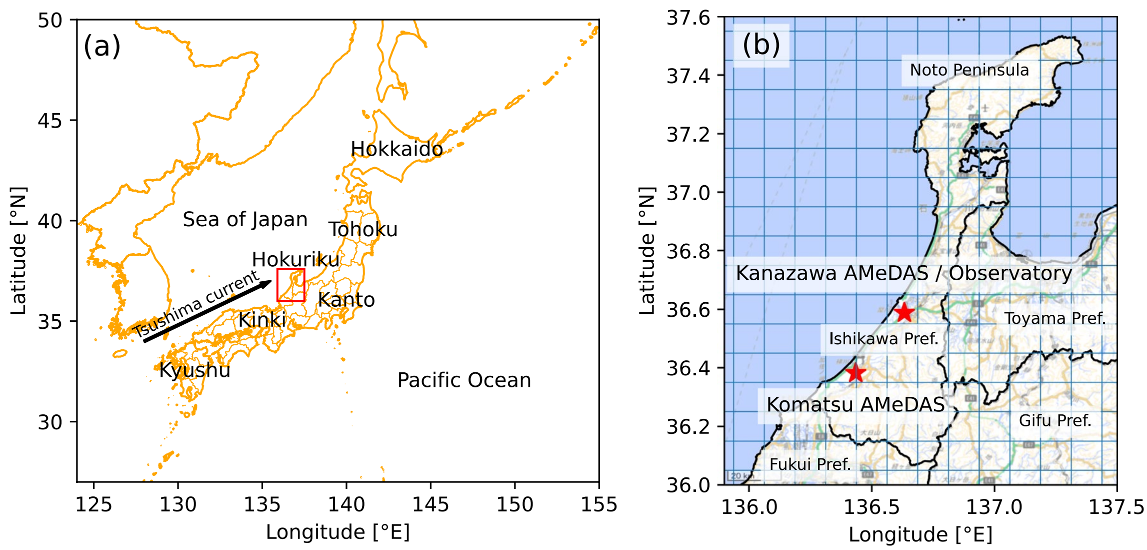

Fig. 1 Maps around Japan and Ishikawa Prefecture. **a** A map of Japan with region names. The red rectangle shows the area shown in the right panel. **b** A map of Ishikawa Prefecture. Red stars show the Kanazawa and Komatsu AMeDAS stations. The Kanazawa local meteorological observatory is located at the same place as the Kanazawa AMeDAS station. The blue mesh indicates the MSM grid. Black lines on the maps are prefectural boundaries

3.1.1 Case 11 (9 January 2018)
In Case 11, 5 gamma-ray glows were detected between 14:00 and 18:00, on 9 January 2018, in Kanazawa and Komatsu. The meteorological charts are shown in Fig. 2. As seen in the surface analysis, there is a developed low with an occluded front at the northeast of Hokkaido, and a low without fronts at Hokkaido. A convex of surface isobaric lines is formed from Kanto toward the low without fronts, and the direction of the surface isobaric lines changes around Hokuriku.

At 500 hPa height, there is a cold-core low at Hokkaido which is associated with the low without fronts. Also, constant-pressure isobaric lines run east and west above the main island of Japan, and a cold-air mass of − 30 °C or colder flows into the Hokuriku region at 500 hPa. When the low-pressure center is northeast of Kanazawa, then the westerly wind around the low (counterclockwise) is present over the warm Sea of Japan, which sets up strong instability and moist convection and brings thunderstorms to the island of Japan.

As seen in the infrared image of the Himawari-8 satellite, there are streak clouds on the Sea of Japan, flowing from the Korean Peninsula to the east to the coastal areas of Japan. In particular, tall convective clouds with a brightness temperature of < −250 K develop on the land of Hokuriku. At the moment of glow detection, the wind blew from west-southwest. The temperature at the surface (measured by AMeDAS) and 850 hPa (provided by MSM) was around 2 °C and − 7 °C, respectively. The − 10 °C altitude calculated with MSM was 1.8 km.

Flash rates are presented in Table 1. No lightning flashes were detected around the detection time of two glows in Komatsu (Events 22 and 23), while 0.2–0.5 flashes per minute in Kanazawa (Events 24–26). The median of the flash rates is 0.2 flashes per minute.

3.1.2 Case 18 (17 December 2018)
In Case 18, 7 gamma-ray glows were detected between 09:00 and 15:00, on 17 December 2018, in Kanazawa. The meteorological charts are shown in Fig. 3. At the surface there is a low with a cold front in the east of Tohoku, going northeast. Also, there is another low without fronts in the northeast of Hokkaido, going northward. There is a convex structure of surface isobaric lines around the Hokuriku region. At 500 hPa, a trough is passing above Hokuriku at the moment of the glow detections, while no cold-core low is detected. Associated with the trough, a cold-air mass of − 24 °C or colder flows into the Hokuriku region.

In the satellite image, there are clouds with a brightness temperature of 250–260 K on the Sea of Japan, and convective clouds with a brightness temperature of < 250 K. At the moment of glow detection, the wind blew from the west. The temperature at the surface and 850 hPa was around 7 °C and − 3 °C, respectively. The − 10 °C altitude was 2.2–2.6 km.

During Events 38–40, there was a relatively active thunderstorm around the detection site, with flash rates of 0.9–1.1 flashes per minute. On the other hand, no lightning flashes were detected during Events 41–44.

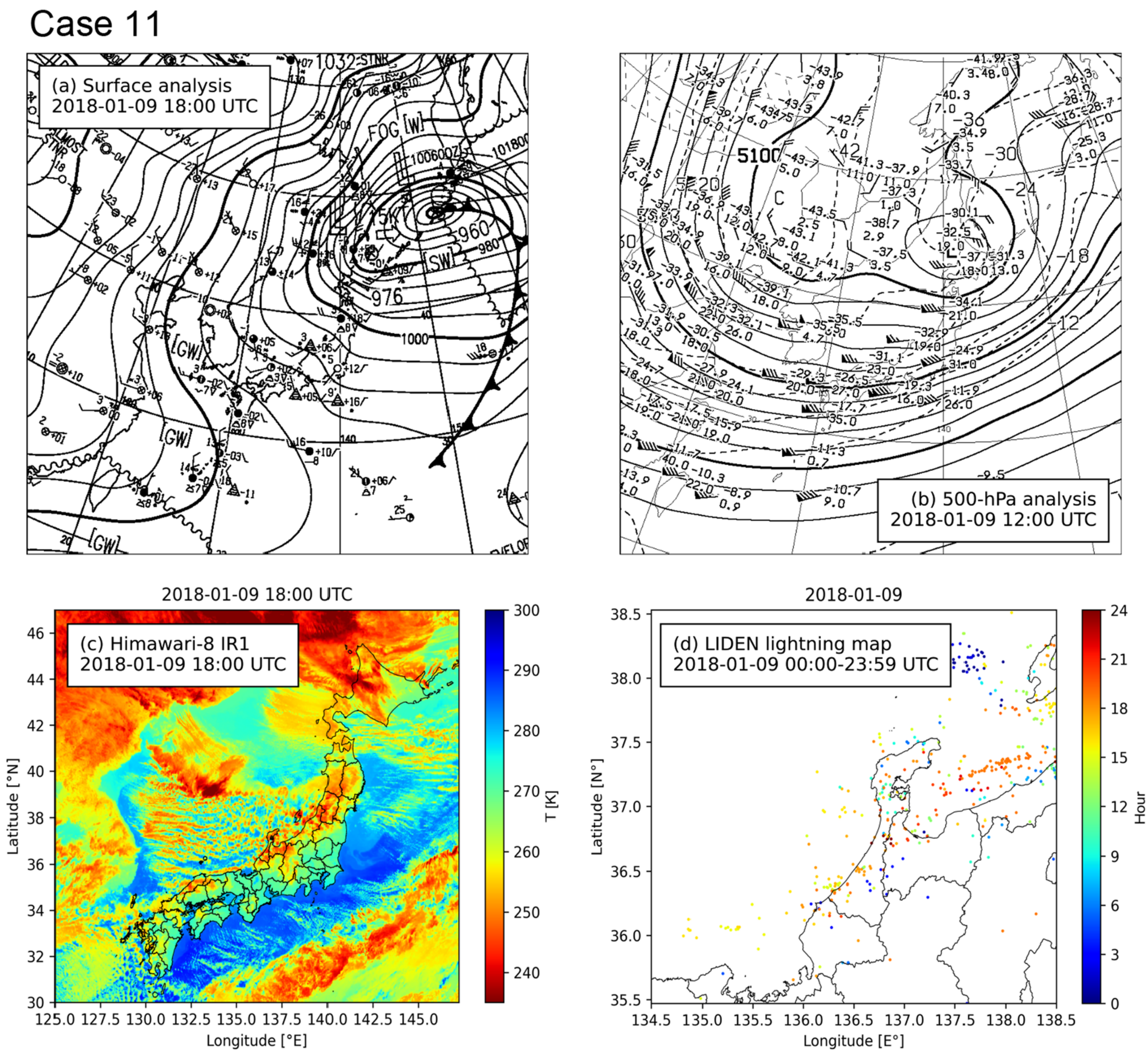

Fig. 2 Meteorological charts of the glow-detection Case 11. **a** An expanded view of JMA surface analysis (ASAS). **b** An expanded view of JMA 500 hPa analysis (AUPQ35). **c** Brightness-temperature heat map taken by Himawari-8 Advanced Himawari Imager IR1 (band 13). **d** Daily lightning map based on the LIDEN observation

3.1.3 Case 19 (18 December 2018)

In Case 19, 6 gamma-ray glows were detected between 14:00 and 15:00, on 18 December 2018, in Kanazawa. This case occurred one day after Case 18. The charts are in Fig. 4. The low without fronts related to Case 18 moved to the north of Sakhalin, and the low with fronts reached the Kamchatka peninsula. The convex structure around Hokuriku is more developed than Case 18.

At 500 hPa, the trough passing above the main island of Japan in Case 18 moved to the east of Japan, and another trough is passing above Hokuriku around 15:00. Also, a cold air mass goes southward, and the temperature at Hokuriku is less than − 30 °C.

Like Case 18, there is a cluster of clouds with a brightness temperature of 250–260 K on the Sea of Japan, and also convective clouds with a brightness temperature of < 250 K on the land of Hokuriku, as seen in the satellite image. The west wind blows, and the surface and 850 hPa temperature is around 7 °C and − 5 °C, respectively. Compared to Case 18, the surface temperature is almost the same, but the 850 hPa temperature is lower. The − 10 °C altitude was 2.2 km.

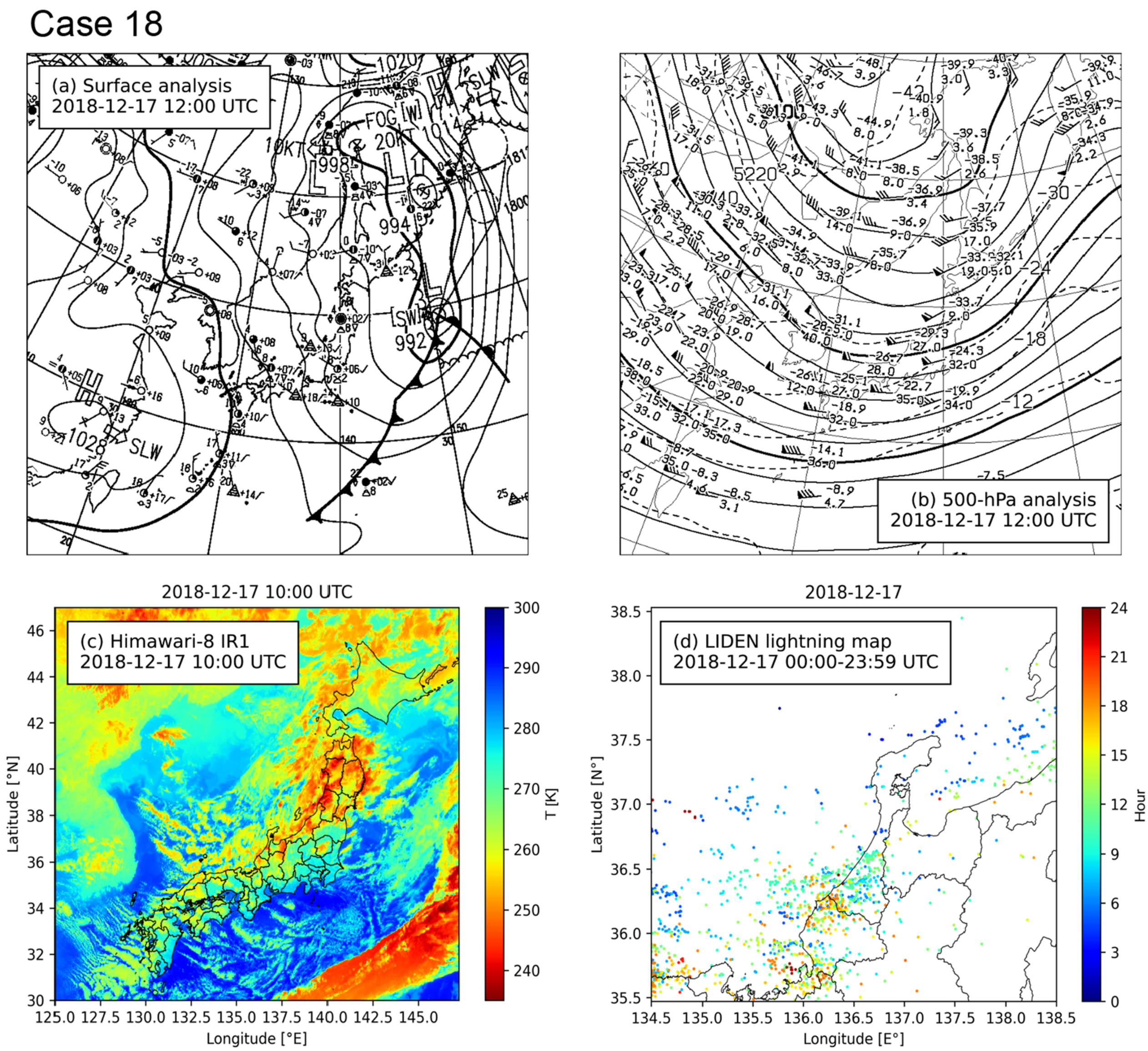

Fig. 3 Meteorological charts of the glow-detection Case 18 in the same format as Fig. 2

The LIDEN lightning map shows that lightning discharges occurred in Ishikawa Prefecture all day. The flash rates are above 1.0 flash per minute, with a median of 1.2 flash per minute. Among the 24 detection cases, this case had the most active thunderstorm during glow detections, based on the flash rates.

3.1.4 Case 23 (17 February 2020)

In Case 23, 11 gamma-ray glows were detected between 11:00 and 17:00, on 17 February 2020. This is the largest number of gamma-ray glows per day in the glow catalog of Wada et al. (2021a). The charts are in Fig. 5. There is a developed low with an occluded front in the east of Hokkaido, and another low without fronts in the west of Hokkaido. At 500 hPa, a cold-core low associated with the low without fronts exists. Since a spiral cluster of convective clouds with a brightness temperature of < 250 K centered at the low is seen in the satellite image, this low is considered to be a polar low.

There is another low without fronts at the surface in the east of Kanto. Also, a convex structure of surface isobaric lines is seen around Hokuriku, as in the three cases above. Isobaric lines at 500 hPa form an ellipse, centered at the polar low. A trough at 500 hPa is passing above Kyushu, yet not above Hokuriku at the moment of glow detection. Tall clouds with a

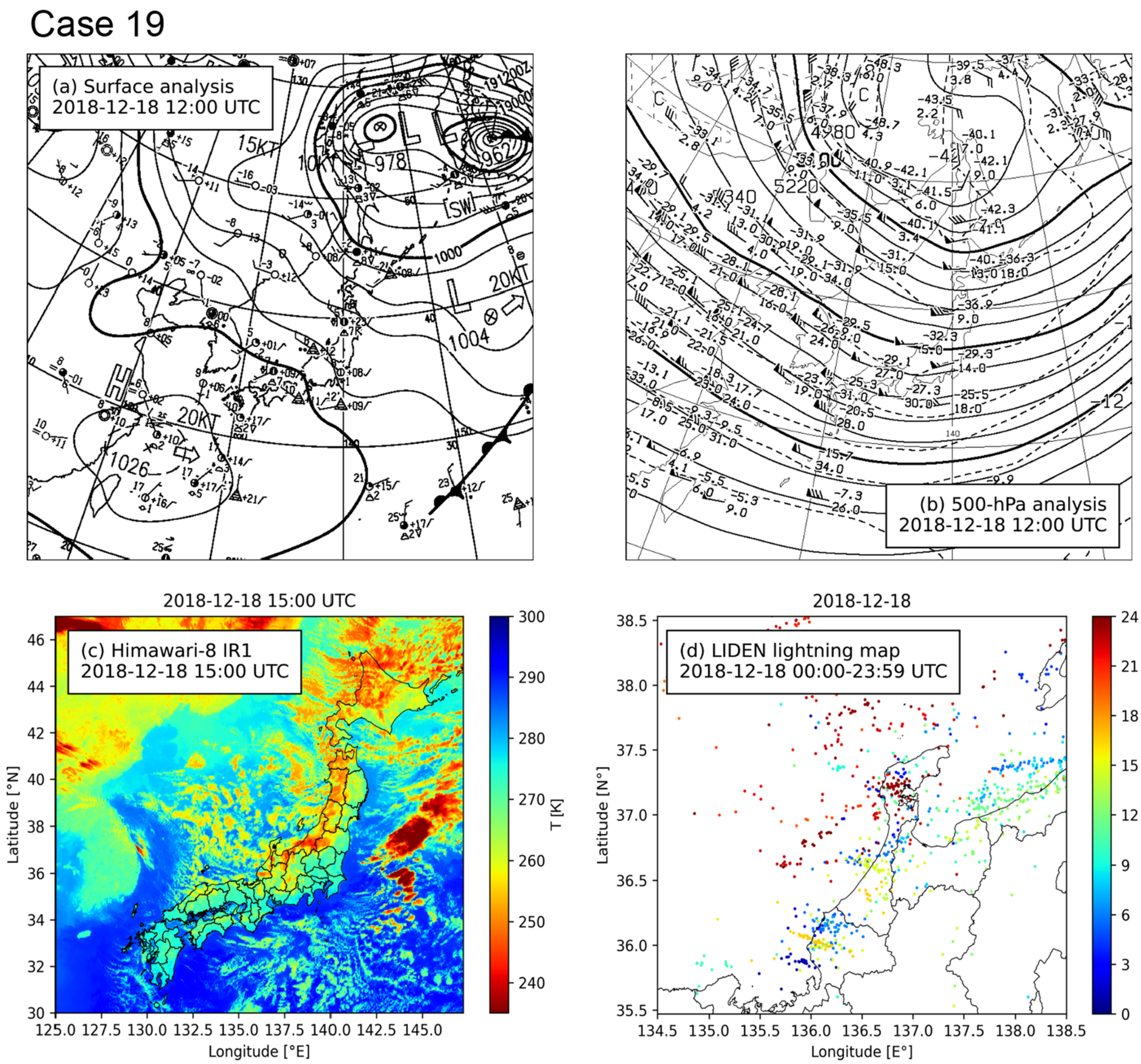

Fig. 4 Meteorological charts of the glow-detection Case 19 in the same format as Fig. 2

brightness temperature of < 240 K form along the isobaric lines at 500 hPa, as seen in the satellite image. In particular, the land of Ishikawa Prefecture is completely covered by convective clouds. At the moment of glow detection, the wind blows from the west or west-southwest. Surface and 850 hPa temperature is around 2 °C and − 7 °C, respectively. The − 10 °C altitude was 1.7–1.8 km.

The lightning activity was quite low. Among 11 glows, no lightning flashes were detected during 7 glows. And the flash rates during the detection of the other glows are 0.2 flashes per minute at most.

3.1.5 Summary of glow-detection cases

We analyze all 24 cases including the four cases described above. The charts of all the cases are uploaded to a data repository (see the Availability of data and material section). Figure 6 shows histograms of surface and 850 hPa temperature, lapse rate, and wind direction for the glow-detection cases. We utilize the median of each value when a glow-detection case includes multiple gamma-ray glows. The average value of surface and 850 hPa temperature, lapse rate, − 10 °C altitude, and wind direction is 4.3 °C, − 5.8 °C, 7.3 °C/km, 2.0 km, and 260°, respectively.

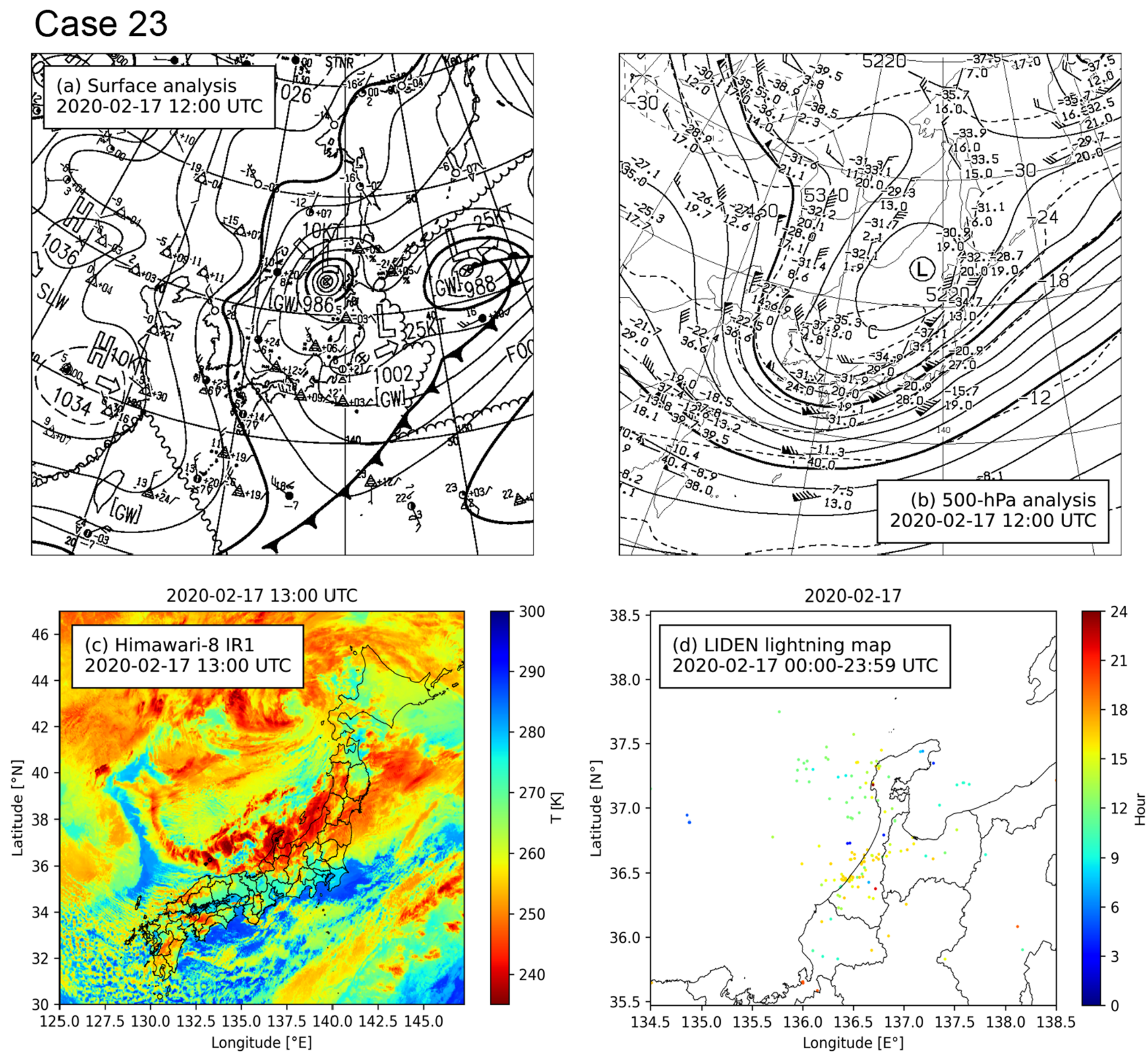

Fig. 5 Meteorological charts of the glow-detection Case 23 in the same format as Fig. 2

The glow-detection cases can be classified into five types. (1) Having a convex structure at the surface around the Hokuriku region (convex type; Cases 1, 3, 6, 8, 9, 11, 12, 16, 17, 18, 19, 20, 22, and 24). (2) Hit by the south edge of a polar low (PL type; Cases 5,10,13,15, and 23). (3) Directly hit by a small low without fronts (small-low type; Cases 7, 14, and 21). (4) A passage of a cold front (cold-front type; Case 2). And (5) Heavy-snow condition (snowy type; Case 4). Most of the cases are classified into the first three types, and the latter two cases are exceptions. This classification, the existence of cold-core lows, the passage of a trough, and a cold front are summarized in Table 2. Cold-core lows exist in 20 of the 24 cases. Besides, the existence of JPCZ that reaches the main island of Japan is investigated based on satellite infrared images, and also, it is tested if Kanazawa is hit by L-mode (longitudinal mode; the cloud strike is parallel to the wind direction), T-mode (transversal mode; the cloud strike is perpendicular to the wind direction), or Cu-Cb (convergence zone between L and T-modes) clouds when JPCZ is confirmed, as in Table 2.

Fourteen cases, the largest number, are classified into the convex type. A typical example is Case 19. There is a high in the southwest of Kyushu and a low in the north of Hokkaido. In the region between the high and low, surface isobaric lines run from northwest to southeast,

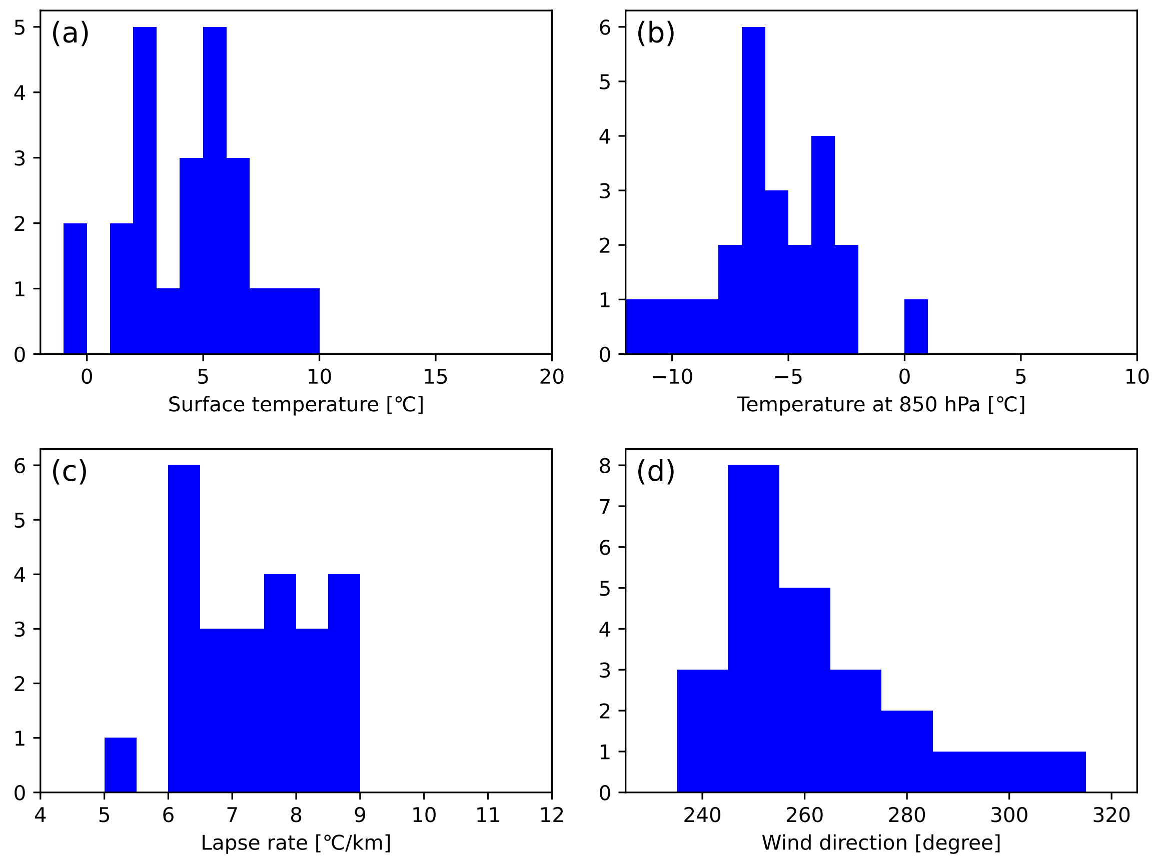

Fig. 6 Histograms of meteorological parameters in the glow-detection cases. **a** Surface temperature measured by AMeDAS stations. **b** The temperature at 850 hPa extracted from MSM. **c** Lapse rate between surface and 850 hPa height calculated with MSM. **d** Wind direction derived with radar images. The wind direction is where the wind comes from clockwise. For example, the direction 270° indicates that wind comes from the west toward the east

but the isobaric lines have a bend and form a convex structure around Hokuriku. This convex structure corresponds to a trough at 500 hPa. The strikes of the isobars at the surface are in the east-west direction on the northwest side of the convex, and hence, westerly wind tends to predominate from the surface to high altitudes around Hokuriku. In many cases, cold-core lows exist, and many correspond to the passage of troughs. There are cases in which a steep trough is passing above as in Case 24, although cold-core lows are not seen. In addition, there are cases where the convex structure is formed due to the effects of multiple lows, even when a trough is not passing, as in Case 16.

Five cases are classified into the PL type. A typical example is Case 5. The charts of Case 5 are shown in Fig. 7. In the satellite image, a cluster of developed clouds is seen in the north of the polar low. Besides, another cluster of streaked and developed clouds is located 500 km south of the polar-low center and covers the Hokuriku region. In fact, lightning strikes are observed along the coast of the Sea of Japan, including the Hokuriku region covered by the streaked clouds, as seen in the LIDEN daily lightning map. Also in other cases, convective clouds that develop along the 500 hPa contour line can be confirmed several hundred kilometers away from the low, apart from developed clouds that developed around the polar low. Isobaric lines at the surface are similar to the convex type.

Three cases are classified into the small-low type. A typical example is Case 7. The charts of Case 7 are shown in Fig. 8. A small low without fronts developed over the Sea of Japan is approaching the Hokuriku region. At this time, in the satellite image, there are developed convective clouds surrounding the low, and it covers the vicinity of Kanazawa. Also in other cases, low-pressure disturbances centered on the Hokuriku region are confirmed by satellite images. At 500 hPa, the cold-core low is confirmed in the north of the small lows in Cases 7 and 21. The passage of troughs at 500 hPa is not clear for the three cases.

Only Case 2 is categorized as the cold-front type. This is one of the two exceptions. The charts are shown

Table 2 List of parameters for glow-detection and non-detection cases

Case no.	Type	Cold-core low	Passage of trough	Passage of cold front	JPCZ (at Kanazawa)	Temperature		Lapse rate (°C/km)	Altitude at − 10 °C (km)	Wind direction (°)	Flash rate (flash/min)
						Ground (°C)	850 hPa (°C)				
1	Convex	No	Yes	No	No	5.9	− 3.2	6.3	2.4	300	0.0
2	Cold-front	Yes	Yes	Yes	No	9.7	0.2	6.7	2.8	260	0.3
3	Convex	Yes	Unclear	No	Yes (L-mode)	5.9	− 5.9	8.8	1.9	265	0.5
4	Snowy	Yes	Yes	No	No	− 0.4	− 11.8	8.4	1.2	310	0.0
5	PL	Yes	Yes	No	Yes (Cu-Cb)	6.8	− 3.8	7.9	2.3	260	0.25
6	Convex	Yes	Yes	No	No	6.8	− 3.8	7.6	2.3	250	0.2
7	Small-low	Yes	No	No	Yes (Cu-Cb)	5.0	− 4.0	6.4	2.2	240	0.2
8	Convex	Yes	Yes	No	Yes (L-mode)	4.9	− 7.1	8.8	1.8	250	0.0
9	Convex	Yes	Unclear	No	No	5.8	− 5.8	8.2	2.0	260	0.0
10	PL	Yes	Unclear	No	No	2.7	− 9.5	8.6	1.5	290	0.1
11	Convex	Yes	No	No	No	2.0	− 6.5	6.3	1.8	250	0.2
12	Convex	Yes	No	No	No	2.2	− 6.1	6.0	1.9	250	0.4
13	PL	Yes	No	No	Yes (Cu-Cb)	− 0.4	− 10.1	6.9	1.4	240	0.2
14	Small-low	Yes	Unclear	No	Yes (Cu-Cb)	1.2	− 7.8	6.2	1.7	260	0.0
15	PL	Yes	Yes	No	No	3.2	− 6.4	7.0	1.8	250	0.0
16	Convex	Yes	No	No	No	1.1	− 8.6	6.9	1.6	250	0.2
17	Convex	Yes	No	No	Yes (L-mode)	5.5	− 6.8	8.4	1.9	250	0.0
18	Convex	No	Yes	No	No	7.7	− 2.2	7.1	2.6	270	0.0
19	Convex	No	Yes	No	No	8.1	− 4.7	8.8	2.2	270	1.2
20	Convex	Yes	No	No	No	4.9	− 5.7	7.5	2.0	275	0.75
21	Small-low	Yes	No	No	No	2.8	− 4.5	5.2	2.1	260	0.1
22	Convex	Yes	Yes	No	No	6.2	− 2.6	6.3	2.5	240	0.6
23	PL	Yes	No	No	Yes (Cu-Cb)	2.6	− 6.9	7.0	1.8	250	0.0
24	Convex	No	Yes	No	No	4.1	− 6.1	7.6	1.8	280	0.3
(Average)						4.3	− 5.8	7.3	2.0	260	0.23
ND1	Convex	Yes	No	No	No	10.5	0.4	7.0	3.0	260	0.1
ND2	Convex	Yes	Yes	No	No	7.6	− 0.6	5.8	2.9	250	0.1
ND3	Convex	Yes	Unclear	No	No	3.4	− 4.8	5.6	2.2	250	0.3
ND4	Quasi-convex	Yes	Yes	No	No	11.0	− 1.8	8.8	2.6	270	0.2
ND5	Cold-front	Yes	Yes	Yes	No	9.2	− 3.2	8.7	2.4	250	0.3
ND6	Cold-front	Yes	Yes	Yes	No	5.5	− 3.5	6.4	2.3	250	0.2
ND7	Convex	Yes	No	No	No	8.8	− 0.8	6.9	2.8	250	0.3
ND8	PL	Yes	Yes	No	No	3.7	− 7.7	8.1	1.7	270	0.2
ND9	Cold-front	No	Yes	Yes	No	5.9	− 3.8	6.8	2.4	260	1.0
ND10	PL	Yes	Yes	No	No	5.2	− 4.1	6.9	2.1	250	0.7
ND11	Cold-front	Yes	Yes	Yes	No	16.1	6.0	7.1	3.8	260	0.2
(Average)						7.9	− 2.2	7.1	2.6	260	0.33

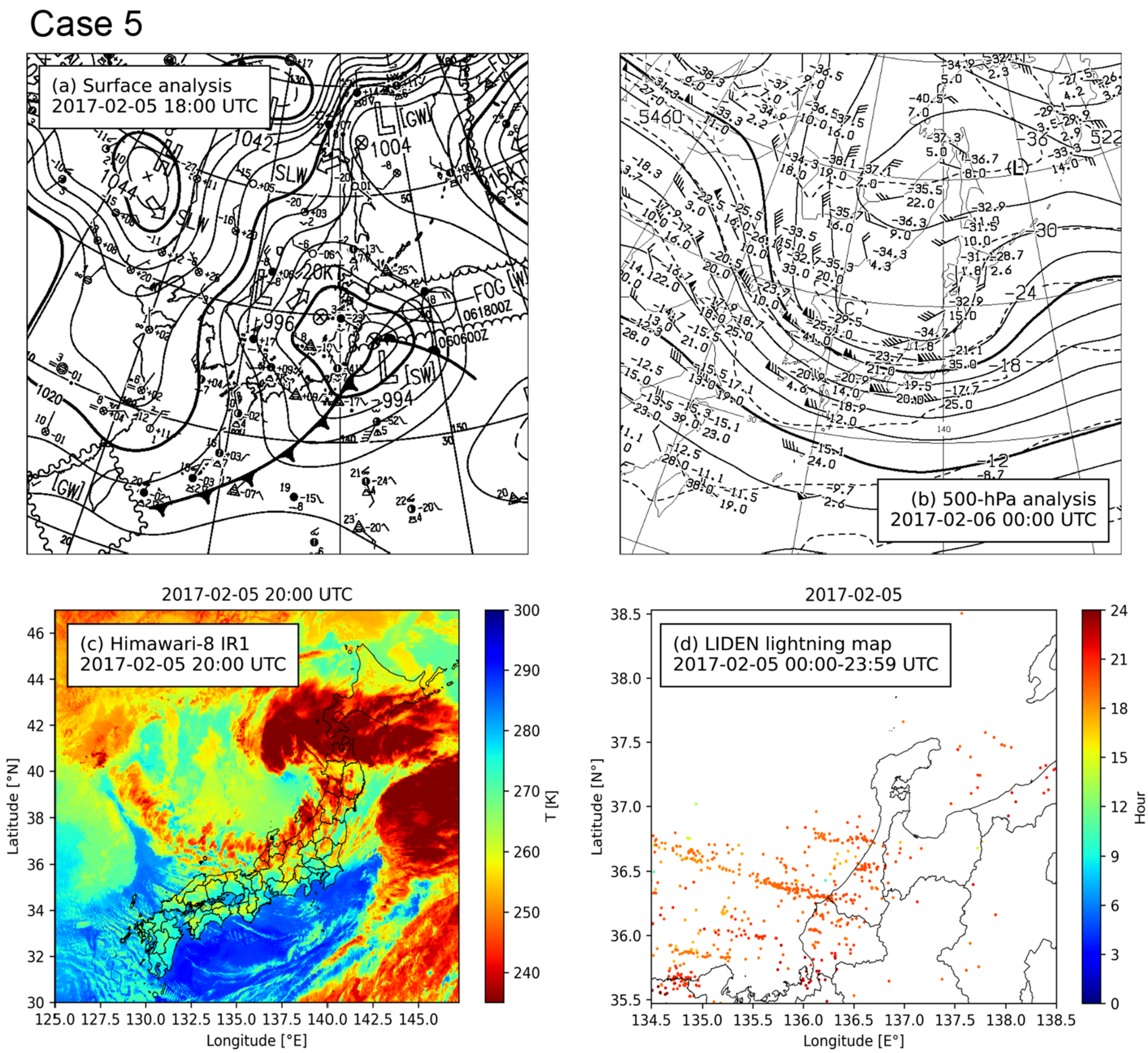

Fig. 7 Meteorological charts of the glow-detection case 5 in the same format as Fig. 2

in Fig. 9. A large number of lightning discharges were observed along the coast of the Sea of Japan as seen in the LIDEN lightning map, but the flash rate around the detection time is relatively low, 0.3 flashes per minute, and only one gamma-ray glow was detected. The cold front at 06:00 has a kink at Ishikawa, indicating that a small low is developing at Ishikawa. At that moment a trough at 500 hPa was passing above.

The other exception is Case 4, classified into the snowy type. The charts are shown in Fig. 10. Surface isobaric lines run from north to south, and there is a cold-core low at 500 hPa in the east of Tohoku. This condition is similar to the mountainous snowfall type, rather than the coastal type. Streaked clouds from the northwest flow into the coast of the Sea of Japan, as seen in the satellite image. At this moment, JMA reported heavy snow in this area. A cold air mass of $< -36\,^{\circ}\mathrm{C}$ flows into the Hokuriku region. Surface and 850 hPa temperature is significantly lower than in other cases, $-0.4\,^{\circ}\mathrm{C}$ and $-11.8\,^{\circ}\mathrm{C}$, respectively. The wind direction at the surface is 310°, which brings cold air into Hokuriku from the northwest. LIDEN reported not many but a few lightning strikes over a wide area along the coast of the Sea of Japan. In fact, no lightning flash was detected around the glow detection by LIDEN.

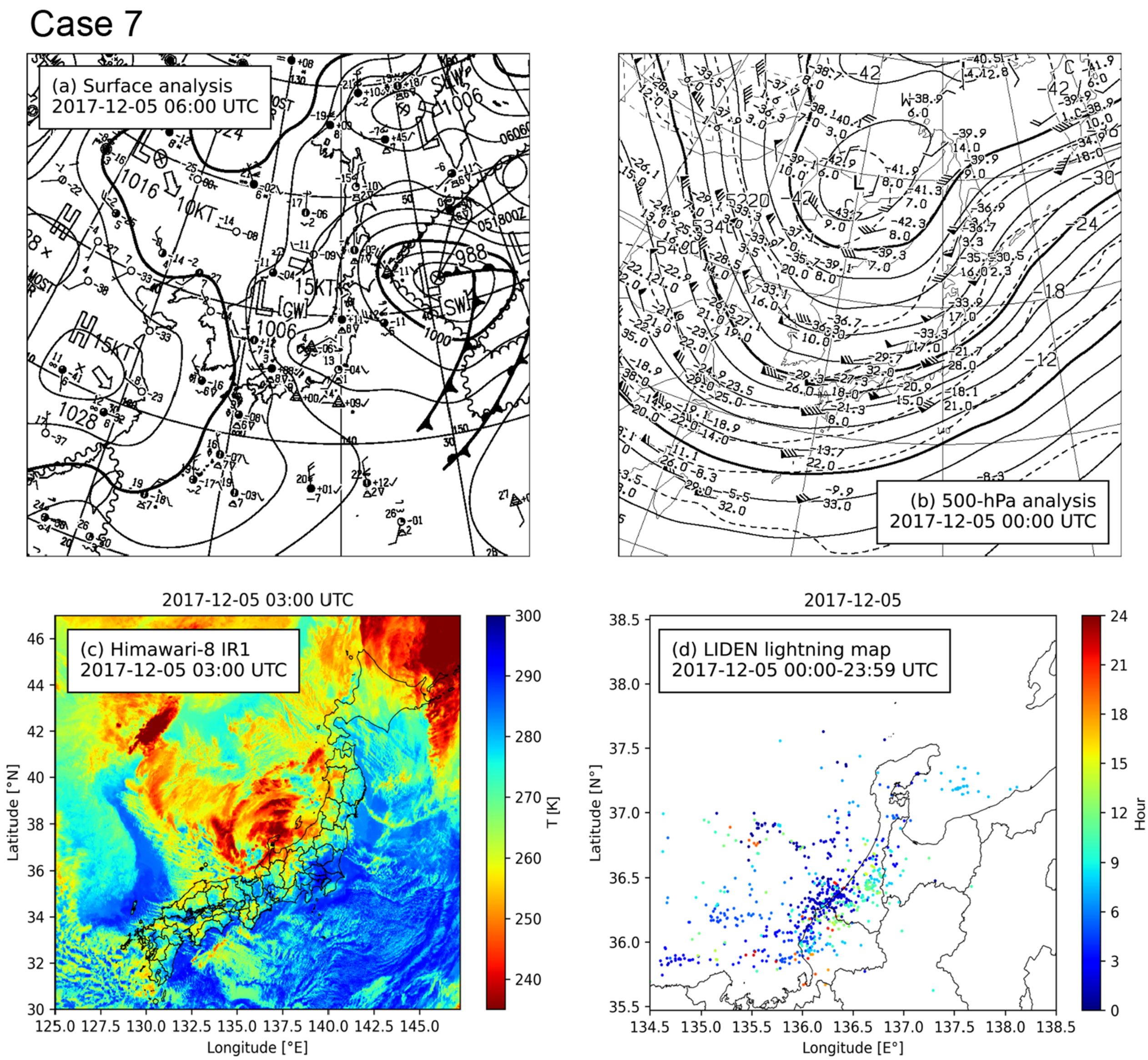

Fig. 8 Meteorological charts of the glow-detection case 7 in the same format as Fig. 2

3.2 Non-detection cases

In order to compare the meteorological conditions between glow-detection and non-detection cases, we extract non-detection cases where gamma-ray glows were not detected even though lightning discharges were occurring around Kanazawa. During the period when gamma-ray monitors of the GROWTH collaboration were in operation, candidate cases in which lightning activities within 10 km from Kanazawa are reported by the Kanazawa local meteorological observatory are selected. The 10 km distance from the Kanazawa local meteorological observatory is set to cover our observation network in Kanazawa. Then, 11 candidates are selected as non-detection cases, in which lightning discharges around Kanazawa are confirmed also by the LIDEN daily lightning maps. The list of the non-detection cases is summarized in Table 3. The maximum flash rates of the non-detection cases vary from 0.1 to 1.0 flashes per minute. The charts of all the non-detection cases are uploaded to a data repository (see the Availability of data and material section). Figure 11 shows histograms of surface and 850 hPa temperature, lapse rate, and wind direction for the non-detection cases. The average value of surface and 850 hPa temperature, lapse rate, − 10 °C altitude, and wind direction is 7.9 °C, − 2.2 °C, 7.1 °C/km, 2.6 km, and 260°, respectively.

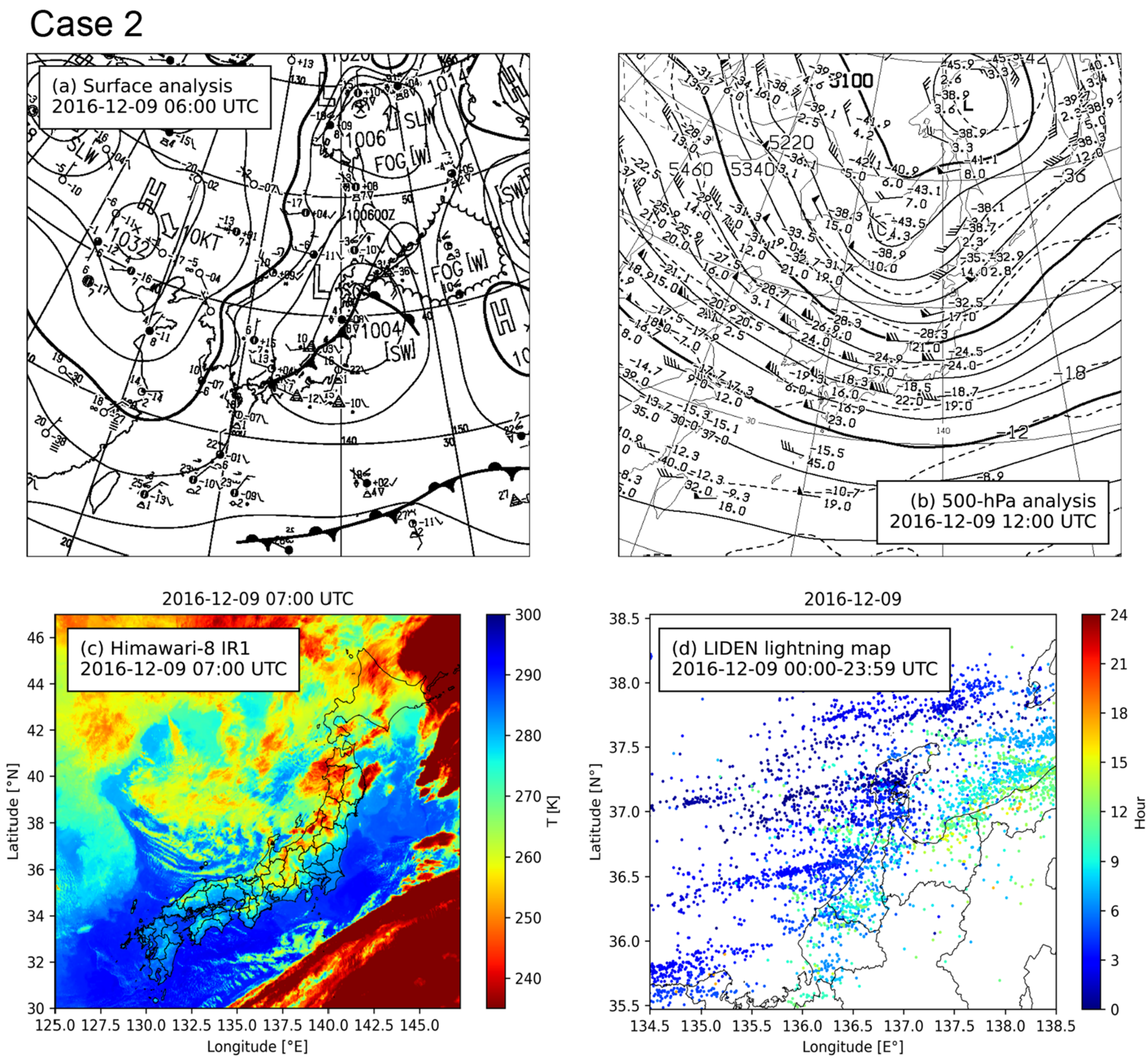

Fig. 9 Meteorological charts of the glow-detection Case 2 in the same format as Fig. 2

The non-detection cases are also classified into four types. Four cases are classified into the convex type (Cases ND1, ND2, ND3, and ND7), four cases into the cold-front type (Cases ND5, ND6, ND9, and ND11), two cases into the PL type (Cases ND8 and ND10), and Case ND4 into a derivative of the convex type (quasi-convex type). Cold-core lows at 500 hPa are confirmed for 10 non-detection cases, except for Case ND9. JPCZ is not confirmed for each case.

In Case ND4, there are two developed lows in the north of Hokkaido, and a corresponding cold-core low is confirmed at 500 hPa. The charts are shown in Fig. 12. On the other hand, an anticyclone is located in the south of Kyushu. The isobars at the surface in the Hokuriku region between the low in the north and the anticyclone in the south run from east to west and are parallel to those at 500 hPa. Although the convex structure was not found in the surface analysis, it is classified as a derivative of the convex type because the wind over the Sea of Japan is considered to be similar to that of the convex type.

4 Discussion

The glow-detection cases are found to be classified into mainly three types (convex, PL, and small-low types), with two exceptions. In particular, the convex type is the most typical condition of gamma-ray glows as 14 of 24

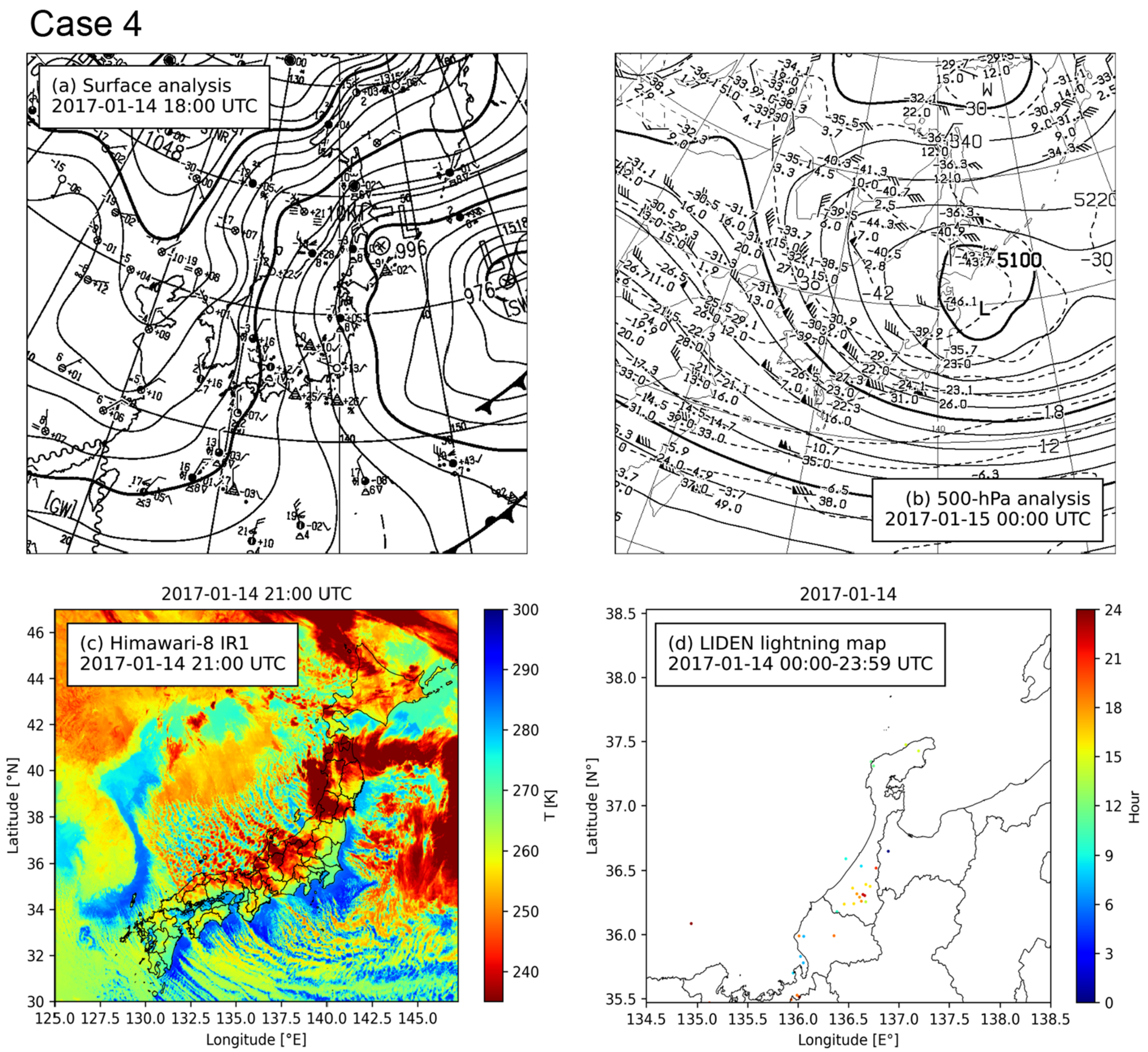

Fig. 10 Meteorological charts of the glow-detection case 4 in the same format as Fig. 2

cases are classified into it. Also, cold-core lows are found in the north of Japan in most of the glow-detection cases. Therefore, convective clouds are considered to be produced by an unstable atmosphere with cold air mass at high altitudes provided by the cold-core lows. A high convective available potential energy (CAPE) value can be observed during winter thunderstorms (Takahashi et al. 2019).

One of the common features between the glow-detection and non-detection cases is that most of both cases occurred when west or west-southwest winds blew at the surface. Fujisawa and Kawamura (2005) reported that west winds with a south component were dominant during winter thunderstorms in the western region of Noto Peninsula (including Ishikawa Prefecture). This report is consistent with the present study. In the PL, small-low, and cold-front types, mesoscale disturbances are considered to provide westerly winds. On the other hand, there are no surface lows nor mesoscale disturbances on the Sea of Japan in some convex-type cases such as Case 19. In these cases, west and southwest winds are thought to dominantly blow along isobars at the surface. West and southwest winds are parallel to the Tsushima warm current, which blows along the coast of the Sea of Japan, and hence, the atmosphere at the surface gets warm and wet before reaching the Hokuriku region.

Table 3 List of non-detection cases in Kanazawa area

Case no.	Period (UTC)	Representative time (UTC)	Temperature		Lapse rate (°C/km)	Altitude at − 10 °C (km)	Wind		Maximum flash rate (flash/min)
			Ground (°C)	850 hPa (°C)			Direction (°)	Speed (m/s)	
1	2017/12/04 05:30-06:20	2017/12/04 06:00	10.5	0.4	7.0	3.0	260	10.4	0.1
2	2017/12/04 12:40-14:00	2017/12/04 13:20	7.6	− 0.6	5.8	2.9	250	11.9	0.1
3	2017/12/18 21:40-00:30	2017/12/18 23:10	3.4	− 4.8	5.6	2.2	250	17.9	0.3
4	2018/12/19 08:20-09:20	2018/12/19 08:50	11.0	− 1.8	8.8	2.6	270	18.8	0.2
5	2019/01/23 11:10-11:20	2019/01/23 11:20	9.2	− 3.2	8.7	2.4	250	16.1	0.3
6	2019/01/28 06:50-07:00	2019/01/28 07:00	5.5	− 3.5	6.4	2.3	250	22.0	0.2
7	2019/03/12 07:40-08:20	2019/03/12 08:00	8.8	− 0.8	6.9	2.8	250	15.6	0.3
8	2019/03/13 10:50-11:10	2019/03/13 11:00	3.7	− 7.7	8.1	1.7	270	17.1	0.2
9	2020/01/19 10:00-11:40	2020/01/19 10:50	5.9	− 3.8	6.8	2.4	260	19.3	1.0
10	2020/03/15 08:40-09:10	2020/03/15 09:00	5.2	− 4.1	6.9	2.1	250	16.3	0.7
11	2020/03/22 00:20-00:50	2020/03/22 00:40	16.1	6.0	7.1	3.8	260	24.9	0.2

Vigorous convections are facilitated between a warm surface atmosphere above the Tsushima current and a cold atmosphere at high altitude (Goto and Narita 1991).

There is no significant difference in flash rates between the glow-detection and non-detection cases. The maximum flash rate in the glow-detection cases is 1.3 flashes per minute around Events 45, 46, and 49 in Case 19. On the other hand, no lightning flashes were detected around 31 glow events among 70. The rates in the non-detection cases are from 0.1 to 1.0 flashes per minute. The average flash rate of the non-detection cases, 0.33 flashes per minute, is larger than that of the glow-detection case, but the maximum one, 1.0 flash per minute, is lower than that of the glow-detection case, 1.3 flashes per minute.

One of the differences between the glow-detection and non-detection case is the temperature at the surface and 850 hPa. While the average temperature at the surface and 850 hPa for the glow-detection cases is 4.3 °C and − 5.8 °C, respectively, that for the non-detection cases is 7.9 °C and − 2.2 °C, respectively. Both temperatures at the surface and 850 hPa in the non-detection cases are 3–4 °C higher than the glow-detection cases. When analyzing individual cases, the surface temperature exceeds 10 °C in Cases ND1, ND4, and ND11, and even the 850 hPa temperature exceeds 0 °C in Cases ND1 and ND11.

The charge structure of thunderclouds is temperature-dependent. Zheng et al. (2019) utilized a lightning mapping array in the very-high-frequency band to investigate winter thunderstorms in Japan and revealed that the main charging process occurred at around or below − 10 °C level. Takahashi et al. (2019) performed sonde observations of charged precipitation particles and documented the temperature-dependent charge structure. In the context of gamma-ray observations, Williams et al. (2022) combined radar and surface electric-field observations with TGE observations in Armenia. They found a clear difference in the vertical structure of radar echoes between TGEs with negative and positive surface electric-field excursions, when the vertical structure is investigated in vertical temperature profiles.

In the non-detection cases with a high-temperature field, the altitude where electrification intensively occurs should get higher than in the other cases. The average temperature at the surface is 4.3 °C and 7.9 °C for the glow-detection and non-detection cases, respectively, with a difference of 3.6 °C. In the same way, the average temperature at the 850 hPa level is − 5.8 °C and − 2.2 °C, respectively, with a difference of 3.6 °C. Assuming a lapse rate of 7 °C/km, the temperature difference of 3.6 °C corresponds to ~ 0.5 km. This difference can be also confirmed by the − 10 °C altitude as the average altitude at − 10 °C of non-detection cases is 0.6 km higher than that of glow-detection cases.

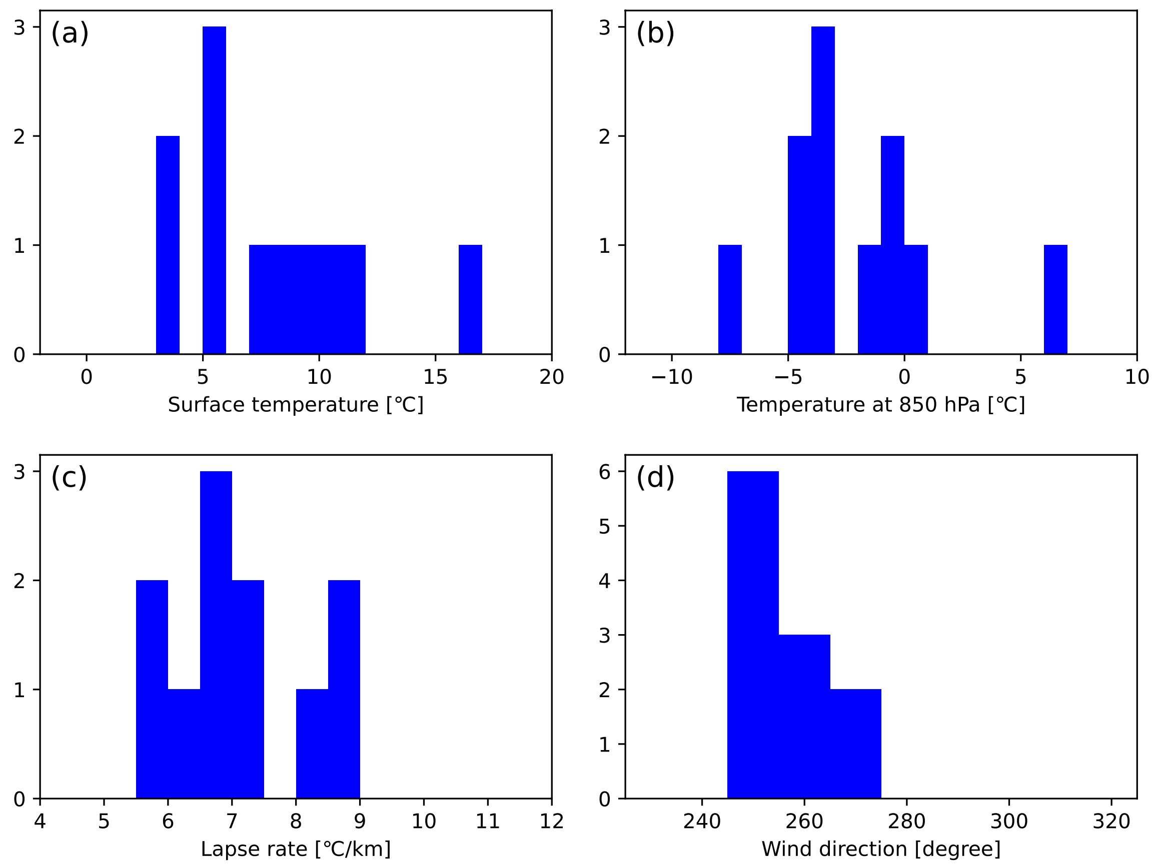

Fig. 11 Histograms of meteorological parameters in the non-detection cases, presented in the same format as Fig. 6

This difference in the distance to the electrified region is critical for photon attenuation in the atmosphere, as the mean free path is 0.22 km for 3 MeV photons, a representative photon energy of gamma-ray glows. Therefore, it will become more difficult to detect gamma-ray glows at sea level in higher temperature fields of the non-detection cases as the altitude where electrons are accelerated and gamma rays are produced gets higher. Except for Case 2, the temperature at 850 hPa is lower than $-2\,°C$ in the glow-detection cases. Therefore, it is considered difficult to observe gamma-ray glows at sea level in Cases ND1, ND2, ND4, ND7, and ND10 even if electron acceleration occurs inside thunderclouds.

The second difference is a direct hit by a small low. In three of the 24 glow-detection cases, a small low without fronts was passing above Ishikawa at the moment of glow detections. On the other hand, there are no non-detection cases of the small-low type. Although the small-low type does not frequently occur, gamma-ray glows tend to be detected once a small-low case occurs.

The third difference is the cold-front type. While only one case among the 24 glow-detection cases is the cold-front type, 4 in 11 non-detection cases are classified into this type. Cold fronts consist of a lower cold layer and a warm layer above, and convection occurs as the warm layer is lifted by running on the cold layer. Therefore, the ambient temperature is relatively high during the passage of cold fronts. The temperatures at 850 hPa of Case 2, ND5, ND6, ND9, and ND11 are higher than the average one of the glow-detection cases. Similar to the first difference, the electrification altitude should be high during the passage of a cold front, making gamma-ray glows difficult to observe on the ground. In Case 2, the cold front had a kink at Ishikawa. It indicates that a small low is developing above Ishikawa. Thus, Case 2 might be a hybrid of the cold-front type and the small-low type. There is no kink nor small lows in the non-detection cases of the cold-front type.

While some non-detection cases have clear differences from the glow-detection cases, there are non-detection cases that have a similar condition to the glow-detection cases. As mentioned above, the mean free path of 3 MeV photons is 0.22 km. This is applicable not only for vertical penetration of photons but also for a horizontal one. It means that gamma-ray glows are detectable roughly within 1 km from their radiation center since gamma rays

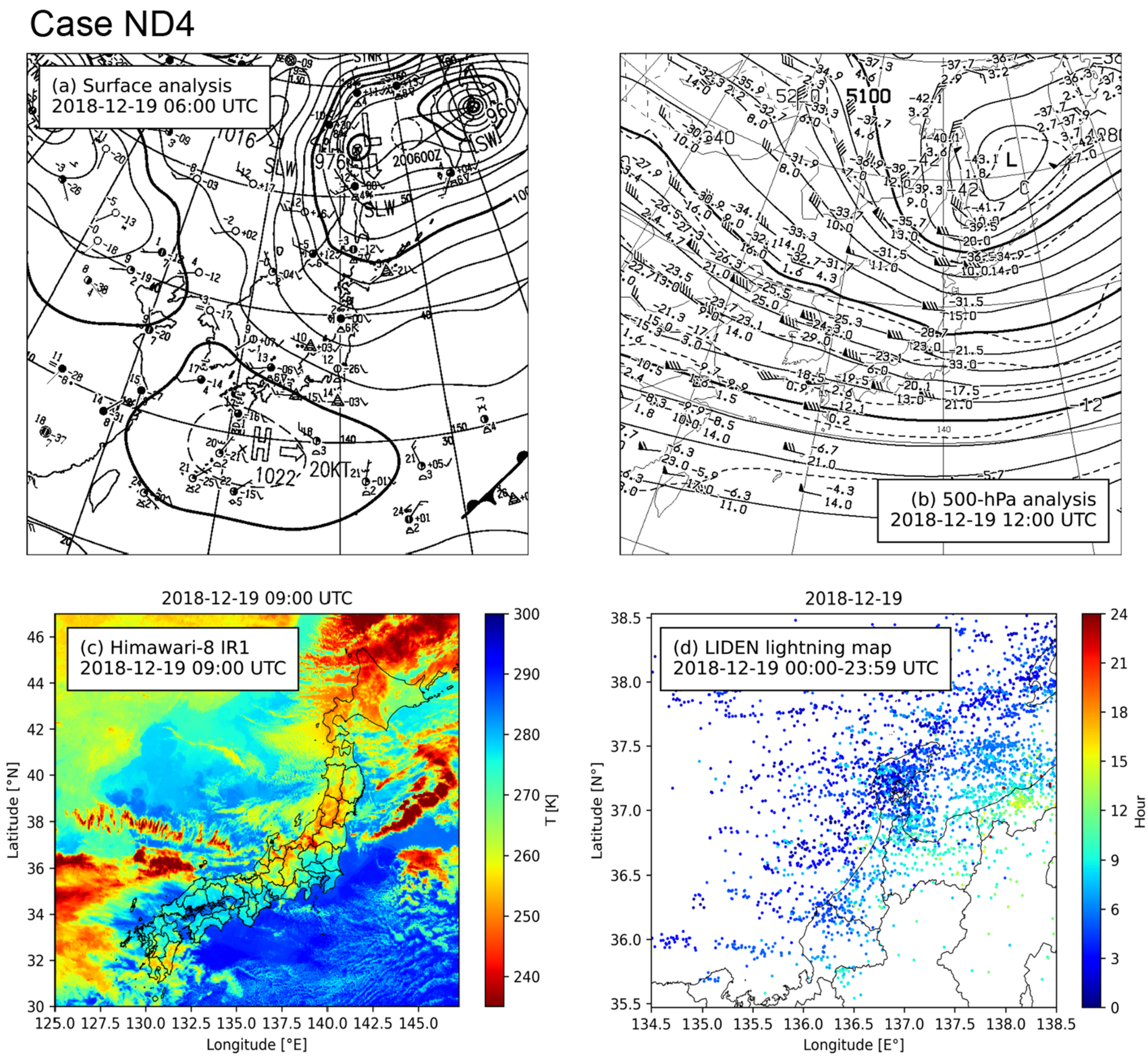

Fig. 12 Meteorological charts of the non-detection case ND4 in the same format as Fig. 2

are attenuated in the atmosphere. Therefore, gamma-ray glows can be only detected when a thundercloud emitting gamma rays is passing directly above detectors. In Cases ND3, ND8, and ND10, whose meteorological conditions are similar to the glow-detection cases, it is possible that gamma-ray glows occurred and were detectable at sea level, but were missed by gamma-ray monitors as the glows did not pass directly above them.

5 Conclusions

In the present study, we investigated synoptic conditions suitable for gamma-ray glow detections at sea level. Twenty-four cases containing 70 gamma-ray glows, detected in the Kanazawa and Komatsu areas by the GROWTH collaboration between December 2016 and March 2020, were classified into three types and two exceptions, based on surface and 500 hPa analyses, MSM, AMeDAS, radar, and satellite observations. Most of the glow-detection cases were categorized as the convex type with curved isobars at the surface, the PL type with a distant polar low, and the small-low type, where a small low directly hits the Hokuriku region. The convex type is the most typical in the glow-detection cases as 14 in 24 are categorized, and most of the convex types are associated with a passage of a trough at 500 hPa. In almost all the cases, the westerly or west-southwest wind was predominant.

In addition, we analyzed 11 non-detection cases between December 2017 and March 2020, in which gamma-ray glows were not detected even though lightning discharges were occurring around Kanazawa. They were classified into the convex type, the PL type, and the cold-front type. Major differences from the glow-detection cases are that more cold-front cases, no small-low cases, higher average temperature both at surface and 850 hPa, and higher altitude at $-10\ ^{\circ}$C. The difference in average temperature, 3.6 °C, corresponds to ~ 0.5 km, which is critical for atmospheric attenuation of gamma rays. Therefore, it would be difficult to detect gamma-ray glows in the cold-front and higher-temperature conditions due to more gamma-ray attenuation in the atmosphere than in the glow-detection cases, while gamma-ray glows are likely detected in a small-low condition. On the other hand, there are some non-detection cases where no significant difference from the glow-detection cases is found. In those cases, gamma-ray glows could have occurred, but thunderclouds emitting gamma rays could have passed far from detectors, and thus, our detection network did not catch them.

Abbreviations

AHI	Advanced Himawari Imager
AMeDAS	Automated Meteorological Data Acquisition System
ASAS	Analysis Surface Asia
AUPQ35	Analysis Upper Western North Pacific 300/500 hPa
GROWTH	Gamma-ray Observation of Winter Thunderclouds
JMA	Japan Meteorological Agency
JPCZ	Japan sea Polar air mass Convergence Zone
JST	Japan Standard Time
LIDEN	LIghtning DEtection Network
MSM	Meso-scale numerical prediction model
ND	Non-detection
PL	Polar low
UTC	Coordinated universal time

Acknowledgements
This work is based on the gamma-ray glow observations performed by the Gamma-Ray Observation of Winter Thunderclouds (GROWTH) collaboration. The datasets and charts produced by Japan Meteorological Agency are provided via Data Integration and Analysis System (DIAS), Certified and Accredited Meteorologists of Japan (CAMJ), Research Institute of Sustainable Humanosphere, Kyoto University, and Center for Environmental Remote Sensing (CEReS), Chiba University

Author contributions
YW leads analysis, discussion, and manuscript drafting. MT contributes to analysis and discussion. SH contributes to LIDEN data curation and discussion. KM contributes to discussion and interpretation. All authors read and approved the final manuscript.

Funding
This work is supported by JSPS KAKENHI Grant Numbers 21H01116 and 22K14453.

Availability of data and materials
The datasets used in this article are available online (https://doi.org/10.17632/2t6n5x986h.2). The MSM and synthetic radar datasets are provided by Japan Meteorological Agency via the Research Institute of Sustainable Humanosphere, Kyoto University (http://database.rish.kyoto-u.ac.jp/arch/jmadata/). XRAIN data are provided by the Ministry of Land, Infrastructure, Transport and Tourism via Data Integration and Analysis System (DIAS). Surface and constant-pressure charts are provided by Japan Meteorological Agency via Certified and Accredited Meteorologists of Japan (CAMJ). Data from the Himawari-8 satellite are provided by Japan Meteorological Agency via Center for Environmental Remote Sensing (CEReS), Chiba University (http://www.cr.chiba-u.jp/japanese/database-himawari.html).

Declarations

Competing interests
The authors declare that they have no competing interests.

Received: 2 June 2022 Accepted: 4 February 2023
Published online: 21 February 2023

References

Asai T (1988) Meso-scale features of heavy snowfalls in Japan sea coastal regions of japan. Tenki 35(3):156–161

Bowers GS, Blaine W, Shao X-M, Dingus B, Smith DM, Schneider M, Martinez-McKinney F, McCarthy MP, BenZvi S, Nellen L et al (2019) Combining Cherenkov and scintillation detector observations with simulations to deduce the nature of high-energy radiation excesses during thunderstorms. Phys Rev D. https://doi.org/10.1103/physrevd.100.043021

Brook M, Nakano M, Krehbiel P, Takeuti T (1982) The electrical structure of the Hokuriku winter thunderstorms. J Geophys Res 87(C2):1207. https://doi.org/10.1029/jc087ic02p01207

Chilingarian A, Daryan A, Arakelyan K, Hovhannisyan A, Mailyan B, Melkumyan L, Hovsepyan G, Chilingaryan S, Reymers A, Vanyan L (2010) Ground-based observations of thunderstorm-correlated fluxes of high-energy electrons, gamma rays, and neutrons. Phys Rev D. https://doi.org/10.1103/physrevd.82.043009

Chilingarian A, Hovsepyan G, Vanyan L (2014) On the origin of the particle fluxes from the thunderclouds: energy spectra analysis. Europhys Lett: EPL 106(5):59001. https://doi.org/10.1209/0295-5075/106/59001

Chilingarian A, Khanikyants Y, Mareev E, Pokhsraryan D, Rakov VA, Soghomonyan S (2017) Types of lightning discharges that abruptly terminate enhanced fluxes of energetic radiation and particles observed at ground level. J Geophys Res Atmos 122(14):7582–7599. https://doi.org/10.1002/2017jd026744

Chilingarian A, Mkrtchyan H, Karapetyan G, Chilingaryan S, Sargsyan B, Arestakesyan A (2019) Catalog of 2017 thunderstorm ground enhancement (TGE) events observed on Aragats. Sci Rep. https://doi.org/10.1038/s41598-019-42786-7

Chilingarian A, Karapetyan T, Zazyan M, Hovsepyan G, Sargsyan B, Nikolova N, Angelov H, Chum J, Langer R (2021) Maximum strength of the atmospheric electric field. Phys Rev D. https://doi.org/10.1103/physrevd.103.043021

Chum J, Langer R, Baše J, Kollárik M, Strhárský I, Diendorfer G, Rusz J (2020) Significant enhancements of secondary cosmic rays and electric field at the high mountain peak of Lomnický Štít in high Tatras during thunderstorms. Earth Planets Space. https://doi.org/10.1186/s40623-020-01155-9

Eito H, Murakami M, Muroi C, Kato T, Hayashi S, Kuroiwa H, Yoshizaki M (2010) The structure and formation mechanism of transversal cloud bands associated with the Japan-sea polar-airmass convergence zone. J Meteorol Soc Jpn Ser II 88(4):625–648. https://doi.org/10.2151/jmsj.2010-402

Fujisawa G, Kawamura R (2005) Recent tendencies of winter thunderstoms in the Hokuriku district and associated atmospheric conditions. Tenki 52(6):449–459

Fujita T (1966) The characteristic of synoptic pattern in heavy snowfall in the coastal and in the mountainous region in Hokuriku district. Tenki 13(10):359–366

Goto Y, Narita K (1991) The meteorological conditions for the occurrence of winter thunderstorms. J Atmos Electr 11(2):61–69. https://doi.org/10.1541/jae.11.61

Gurevich AV, Milikh GM, Roussel-Dupre R (1992) Runaway electron mechanism of air breakdown and preconditioning during a thunderstorm. Phys Lett A 165(5–6):463–468. https://doi.org/10.1016/0375-9601(92)90348-p
Ishii K, Hayashi S, Fujibe F (2014) Statistical analysis of temporal and spatial distributions of cloud-to-ground lightning in Japan from 2002 to 2008. J Atmos Electr 34(2):79–86. https://doi.org/10.1541/jae.34.79
Iwamoto K, Nakai S, Sato A (2008) Statistical analyses of snowfall distribution in the Niigata area and its relationship to the wind distribution. SOLA 4:45–48. https://doi.org/10.2151/sola.2008-012
Kitagawa N (1992) Charge distribution of winter thunderclouds. Res Lett Atmos Electr 12:143–153
Kitagawa N, Michimoto K (1994) Meteorological and electrical aspects of winter thunderclouds. J Geophys Res 99(D5):10713. https://doi.org/10.1029/94jd00288
Kuroda Y, Oguri S, Kato Y, Nakata R, Inoue Y, Ito C, Minowa M (2016) Observation of gamma ray bursts at ground level under the thunderclouds. Phys Lett B 758:286–291. https://doi.org/10.1016/j.physletb.2016.05.029
McCarthy M, Parks GK (1985) Further observations of x-rays inside thunderstorms. Geophys Res Lett 12(6):393–396. https://doi.org/10.1029/gl012i006p00393
Michimoto K (1993) A study of radar echoes and their relation to lightning discharges of thunderclouds in the Hokuriku district. J Meteorol Soc Jpn Ser II 71(2):195–204
Miyake K, Suzuki T, Takashima M, Takuma M, Tada T (1990) Winter lightning on Japan sea coast-lightning striking frequency to tall structures. IEEE Trans Power Deliv 5(3):1370–1376. https://doi.org/10.1109/61.57979
Parks GK, Mauk BH, Spiger R, Chin J (1981) X-ray enhancements detected during thunderstorm and lightning activities. Geophys Res Lett 8(11):1176–1179. https://doi.org/10.1029/gl008i011p01176
Rakov VA, Uman MA (2003) Lightning: physics and effects. Cambridge University Press, Cambridge
Shepetov A, Antonova V, Kalikulov O, Kryakunova O, Karashtin A, Lutsenko V, Mamina S, Mukashev K, Piscal V, Ptitsyn M, Ryabov V, Sadykov T, Saduev N, Salikhov N, Shlyugaev Y, Vildanova L, Zhukov V, Gurevich A (2021) The prolonged gamma ray enhancement and the short radiation burst events observed in thunderstorms at Tien Shan. Atmos Res 248:105266. https://doi.org/10.1016/j.atmosres.2020.105266
Suzuki T (1992) Long term observation of winter lightning on japan sea coast. Res Lett Atmos Electr 12:53–56
Tachibana Y, Honda M, Nishikawa H, Kawase H, Yamanaka H, Hata D, Kashino Y (2022) High moisture confluence in Japan sea polar air mass convergence zone captured by hourly radiosonde launches from a ship. Sci Rep. https://doi.org/10.1038/s41598-022-23371-x
Takahashi T, Sugimoto S, Kawano T, Suzuki K (2019) Microphysical structure and lightning initiation in Hokuriku winter clouds. J Geophys Res Atmos 124(23):13156–13181. https://doi.org/10.1029/2018jd030227
Takenaka H, Sakashita T, Higuchi A, Nakajima T (2020) Geolocation correction for geostationary satellite observations by a phase-only correlation method using a visible channel. Remote Sens 12(15):2472. https://doi.org/10.3390/rs12152472
Takeuti T, Nakano M, Brook M, Raymond DJ, Krehbiel P (1978) The anomalous winter thunderstorms of the Hokuriku coast. J Geophys Res 83(C5):2385. https://doi.org/10.1029/jc083ic05p02385
Torii T, Takeishi M, Hosono T (2002) Observation of gamma-ray dose increase associated with winter thunderstorm and lightning activity. J Geophys Res Atmos 107(D17):2–1213. https://doi.org/10.1029/2001jd000938
Torii T, Sugita T, Tanabe S, Kimura Y, Kamogawa M, Yajima K, Yasuda H (2009) Gradual increase of energetic radiation associated with thunderstorm activity at the top of Mt. Fuji. Geophys Res Lett. https://doi.org/10.1029/2008gl037105
Tsuchiya H, Enoto T, Yamada S, Yuasa T, Kawaharada M, Kitaguchi T, Kokubun M, Kato H, Okano M, Nakamura S et al (2007) Detection of high-energy gamma rays from winter thunderclouds. Phys Rev Lett. https://doi.org/10.1103/physrevlett.99.165002
Tsuchiya H, Enoto T, Torii T, Nakazawa K, Yuasa T, Torii S, Fukuyama T, Yamaguchi T, Kato H, Okano M et al (2009) Observation of an energetic radiation burst from mountain-top thunderclouds. Phys Rev Lett. https://doi.org/10.1103/physrevlett.102.255003
Tsuchiya H, Enoto T, Yamada S, Yuasa T, Nakazawa K, Kitaguchi T, Kawaharada M, Kokubun M, Kato H, Okano M et al (2011) Long-duration γ ray emissions from 2007 and 2008 winter thunderstorms. J Geophys Res. https://doi.org/10.1029/2010jd015161
Tsuchiya H, Hibino K, Kawata K, Hotta N, Tateyama N, Ohnishi M, Takita M, Chen D, Huang J, Miyasaka M et al (2012) Observation of thundercloud-related gamma rays and neutrons in Tibet. Phys Rev D. https://doi.org/10.1103/physrevd.85.092006
Tsuchiya H, Enoto T, Iwata K, Yamada S, Yuasa T, Kitaguchi T, Kawaharada M, Nakazawa K, Kokubun M, Kato H et al (2013) Hardening and termination of long-duration γ rays detected prior to lightning. Phys Rev Lett. https://doi.org/10.1103/physrevlett.111.015001
Wada Y, Bowers GS, Enoto T, Kamogawa M, Nakamura Y, Morimoto T, Smith DM, Furuta Y, Nakazawa K, Yuasa T et al (2018) Termination of electron acceleration in thundercloud by intracloud/intercloud discharge. Geophys Res Lett 45(11):5700–5707. https://doi.org/10.1029/2018gl077784
Wada Y, Enoto T, Nakamura Y, Furuta Y, Yuasa T, Nakazawa K, Morimoto T, Sato M, Matsumoto T, Yonetoku D, Sawano T, Sakai H, Kamogawa M, Ushio T, Makishima K, Tsuchiya H (2019) Gamma-ray glow preceding downward terrestrial gamma-ray flash. Commun Phys 2(1):67. https://doi.org/10.1038/s42005-019-0168-y
Wada Y, Matsumoto T, Enoto T, Nakazawa K, Yuasa T, Furuta Y, Yonetoku D, Sawano T, Okada G, Nanto H, Hisadomi S, Tsuji Y, Diniz GS, Makishima K, Tsuchiya H (2021a) Catalog of gamma-ray glows during four winter seasons in Japan. Phys Rev Res. https://doi.org/10.1103/physrevresearch.3.043117
Wada Y, Enoto T, Kubo M, Nakazawa K, Shinoda T, Yonetoku D, Sawano T, Yuasa T, Ushio T, Sato Y, Diniz GS, Tsuchiya H (2021b) Meteorological aspects of gamma-ray glows in winter thunderstorms. Geophys Res Lett. https://doi.org/10.1029/2020gl091910
Williams E, Mkrtchyan H, Mailyan B, Karapetyan G, Hovakimyan S (2022) Radar diagnosis of the thundercloud electron accelerator. J Geophys Res Atmos. https://doi.org/10.1029/2021jd035957
Yamamoto Y, Ichii K, Higuchi A, Takenaka H (2020) Geolocation accuracy assessment of Himawari-8/AHI imagery for application to terrestrial monitoring. Remote Sens 12(9):1372. https://doi.org/10.3390/rs12091372
Yoshida S, Morimoto T, Ushio T, Kawasaki Z-I, Torii T, Wang D, Takagi N, Watanabe T (2008) High energy photon and electron bursts associated with upward lightning strokes. Geophys Res Lett. https://doi.org/10.1029/2007gl032438
Yuasa T, Wada Y, Enoto T, Furuta Y, Tsuchiya H, Hisadomi S, Tsuji Y, Okuda K, Matsumoto T, Nakazawa K, Makishima K, Miyake S, Ikkatai Y (2020) Thundercloud project: Exploring high-energy phenomena in thundercloud and lightning. Progress Theor Exp Phys. https://doi.org/10.1093/ptep/ptaa115
Zheng D, Wang D, Zhang Y, Wu T, Takagi N (2019) Charge regions indicated by LMA lightning flashes in Hokuriku's winter thunderstorms. J Geophys Res Atmos. https://doi.org/10.1029/2018jd030060